HEEGAARD FLOER HOMOLOGY

by

Taylan Bilal

A Thesis Submitted to the
Graduate School of Arts & Sciences
in Partial Fulfillment of the Requirements for
the Degree of

Master of Science

in

Mathematics

Koç University

August, 2008

Koç University

Graduate School of Sciences and Engineering

This is to certify that I have examined this copy of a master's thesis by

Taylan Bilal

and have found that it is complete and satisfactory in all respects,
and that any and all revisions required by the final
examining committee have been made.

Committee Members:

_____

Assoc. Prof. Tolga Etgü

_____

Assoc. Prof. Burak Özbağcı

_____

Assist. Prof. Ferit Öztürk

Date: _____

To Mazhar Kerestecioğlu, Nurten Kerestecioğlu, Süleyman Bilal and Emine Bilal

ABSTRACT

P. Ozsváth and Z. Szabó recently introduced Heegaard Floer homology, an invariant for closed oriented 3-manifolds associating to each such manifold a sequence of finitely generated abelian groups. The construction has also been extended to an invariant for knots, and then for links.

The definition of Heegaard Floer homology involves many steps, such as Heegaard decompositions and pointed Heegaard diagrams of 3-manifolds, symmetric products of surfaces and counting some holomorphic representatives of disks on the symmetric product. Certain variations concerning these steps lead to four different types of homologies.

With additional basepoints in the Heegaard diagram, one can obtain knots or links in a 3-manifold and consequently the Heegaard Floer homologies become invariants for knots and links. They are called knot (or link) Floer homologies. In this thesis, only knots and links in the 3-sphere are studied, but it should be noted that the ideas are applicable for knots and links in an arbitrary closed oriented 3-manifold.

In the final chapter, we analyze a combinatorial way of computing knot and link Floer homologies, due to C. Manolescu, P. Ozsváth, and S. Sarkar. The idea is to use some special Heegaard diagrams, in order to project the knot to a grid diagram and compute the differential map in a purely combinatorial way. We also include computations of knot Floer homologies for the trefoil and the figure eight knot with the help of the MATLAB software.

ÖZETÇE

Heegaard Floer homolojisi, yakın geçmişte ortaya çıkan, kapalı ve yönlü 3-çokkatlılara sonlu üreteçli değişmeli grup dizisi eşleyen bir değişmezdir. Kullanılan yapılar düğüm ve zincirler için de genişletilebilir.

Heegaard Floer homolojisinin tanımlanması birçok teknik detay gerektirmektedir. Bunlardan bazıları bir 3-çokkatlının Heegaard ayrışımları ve Heegaard diyagramları, yüzeylerin simetrik çarpımları ve bu simetrik çarpım uzaylarında birtakım disklerin holomorfik temsillerinin sayılmasıdır. Bu işlemlerin bazılarında yapılacak küçük değişiklikler, farkli homoloji çeşitlerinin tanımlanmasına olanak tanır.

Bu yapılara birkaç ek veri ekleyerek, bir 3-çokkatlının içerisinde düğüm ve zincirler belirlenebilir. Böylece, yukarıda bahsi geçen yapılar düğüm ve zincirler için değişmezler olurlar. Bunlara düğüm (veya zincir) Floer homolojileri adı verilir. Bu çalışmada sadece 3 boyutlu küredeki düğüm ve zincirler incelenmiştir, ancak yapılanlar genel kapalı ve yönlü 3-çokkatlılar için de geçerlidir.

Son bölümde ise, bazı özel Heegaard diyagramları kullanılarak, düğüm ve zincir Floer homolojilerine kombinatoryal bir bakış açısı sunulmuştur. Ayrıca, yonca ve sekiz şekli düğümlerinin homoloji gruplarına dair hesaplar yapılmıştır.

ACKNOWLEDGMENTS

I would like to thank first my supervisor Assoc. Prof. Tolga Etgü for accepting me as his student, and his wise and balanced approach throughout my studies. He has been a great source of inspiration. I also thank the professors in my thesis committee Assoc. Prof. Burak Özbağcı and Assist. Prof. Ferit Öztürk for carefully examining my work.

I should express that I am grateful to my parents and my grandparents for their support, not just during my thesis work but my entire life. I am also thankful to my girlfriend İlke Bereketli, my room mates Buğra Toga, İlker Ocaklı, Murat Senan, Tarkan Güçlü, Emre Kalafatlar, and my friends Habiba Kalantarova, Cihan Bilir, Zekiye Şahin, Ramazan Erduran, Barış Tümerkan and Eren Büyükevin (special thanks go to the last two for the computer support) who all made the Koç University experience much more enjoyable.

Finally, I would like to express my gratitude to Professors Ali Ülger, Varga Kalantarov, Burak Erman and Mine Çağlar and any other people who all eased my way in switching from Computational Sciences and Engineering department to Mathematics.

TABLE OF CONTENTS

LIST OF TABLES

LIST OF FIGURES

NOMENCLATURE

Σ	Heegaard surface
$\widehat{CF}, CF^\infty, CF^+, CF^-$	Heegaard Floer chain complexes
$\widehat{HF}, HF^\infty, HF^+, HF^-$	Heegaard Floer homologies
$\widehat{HFK}, HFK^-$	Knot Floer homologies
$\widehat{HFL}, HFL^\infty$	Link Floer homologies
$HFL^-_m, HFL'_m\widehat{HFL}_m$	Link Floer homologies with multiple basepoints
Γ	Grid diagram

Chapter 1

INTRODUCTION

Floer initially introduced the "Floer homology" in order to study some problems in Hamiltonian dynamics, and used it in his proof of Arnold conjecture in symplectic geometry [12]. Since then, various adaptations of Floer homology emerged, such as "Instanton Floer homology", "monopole Floer homology", and finally "Heegaard Floer homology".

Heegaard Floer homology is an invariant for closed oriented 3-manifolds, recently introduced by Peter S. Ozsváth and Zoltán Szabó in [16]. It is conjecturally equivalent to Seiberg-Witten theory [11]. Some of the applications of Heegaard Floer homology include knot and link invariants, invariants for 3-manifolds with boundary and also 4-manifolds, and certain results in contact geometry [13].

We will initially review the definition of the Heegaard Floer homology for a closed orientable 3-manifold, and later knot Floer and link Floer homologies for knots and links in S^3. Once we define these invariants, a combinatorial description of link Floer homology will be reviewed, along with some examples.

In Chapter 2, we proceed into the preliminaries and the other steps which are necessary for defining the Heegaard Floer homology. We first explain Heegaard decompositions and (pointed) Heegaard diagrams of 3-manifolds. Then we will focus on the symmetric product of the Heegaard surface (the surface arising from the Heegaard decomposition). Using this symmetric product, we define the generators of a graded chain complex and homotopy classes of the disks connecting these generators. A crucial ingredient in defining the differential map of the chain complex is counting the pseudo-holomorphic representatives of those disks which have zero dimensional moduli space of representatives (after modding out a certain $\mathbb{R}$-action). In the final section of Chapter 2, we define four types of Heegaard Floer homologies for rational homology spheres, all obtained in similar ways, with only small differences in the way they count the disks connecting the generators.

In Chapter 3, we review the modification of the construction by adding more (an even number of) basepoints into the Heegaard diagram and dividing them into pairwise disjoint subsets each containing two points. Every such subset determines a knot, and consequently the constructions of Chapter 2 induce a knot or link (based on the number of basepoints in the diagram) invariant. This is called knot or link Floer homology. In this case, we have also a filtration on the chain complex. We present two different versions of knot and link Floer homologies. Finally, the Heegaard diagrams are modified further to define "link Floer homology with multiple basepoints" to be used in the definition of combinatorial link Floer homology afterwards.

In the final chapter, we review an algorithm of C. Manolescu, P. Ozsváth, and S. Sarkar [8], which computes knot and link Floer homology. Unfortunately this algorithm comes with a high computational complexity. This combinatorial approach can be considered independent from the previous subjects, since it can be defined purely combinatorially without making reference to any of the previous constructions. Nevertheless, we tried to stress the relations between combinatorial and classical approaches in the text.

We also included computations of combinatorial knot Floer homology for the trefoil and the figure eight knot. The complexity of the algorithm required computer assistance, for which we made use of the software MATLAB. The code is available in the CD version of this thesis, or via e-mail (taylanbil@gmail.com).

Chapter 2

HEEGAARD FLOER HOMOLOGY

Heegaard Floer homology is a closed oriented 3-manifold invariant, associating to each such manifold Y a chain of finitely generated abelian groups. It has four most common versions, denoted by $\widehat{HF}(Y), HF^{\infty}(Y), HF^{+}(Y), HF^{-}(Y)$. Many constructions will be needed in order to define this homology, such as Heegaard decompositions of 3-manifolds, symmetric products of surfaces, *spin*^{c}-structures, Maslov index, etc.

From now on, Y will denote a closed, oriented, connected 3-manifold unless otherwise stated.

2.1 Preliminaries

In this section we will give the preliminaries necessary for the definition of the Heegaard Floer homologies.

2.1.1 Heegaard Decompositions and Heegaard Diagrams

A 3-manifold U is said to be a *genus g handlebody* whenever it is diffeomorphic to some regular neighborhood of a bouquet of g circles in $\mathbb{R}^3$. Observe that the boundary of U is a closed oriented surface of genus g. Heegaard decomposition of a 3-manifold Y uses the idea of obtaining the manifold Y by gluing two genus g handlebodies along their common boundary. Namely, whenever we have

$$Y = U_0 \cup_{\Sigma} U_1 \tag{2.1}$$

where U_0, U_1 are genus g handlebodies and Σ is their common boundary, this is called a genus g Heegaard decomposition of the manifold Y. Observe that the same manifold Y can have many different Heegaard decompositions. More specifically, two decompositions of Y may have different genera, conversely, two decompositions of Y with same genus are not necessarily identical. Note that Σ will be called the "Heegaard surface" associated to the decomposition.

A Heegaard diagram associated to a Heegaard decomposition is a triplet $(\Sigma, \boldsymbol{\alpha}, \boldsymbol{\beta})$ where Σ is a Heegaard surface of genus g, and $\boldsymbol{\alpha}$, $\boldsymbol{\beta}$ are g-tuples of simple closed curves (i.e. $\boldsymbol{\alpha} = (\alpha_1, \ldots, \alpha_g)$, $\boldsymbol{\beta} = (\beta_1, \ldots, \beta_g)$ for some simple closed curves α_i's and β_j's) embedded in Σ, satisfying the following:

- $\alpha_i \cap \alpha_j = \beta_i \cap \beta_j = \emptyset$ for all distinct i, j's
- $[\alpha_i]$'s are linearly independent in $H_1(\Sigma, \mathbb{Z})$
- $[\beta_i]$'s are linearly independent in $H_1(\Sigma, \mathbb{Z})$
- α_i's bound disjoint embedded disks in U_0
- β_i's bound disjoint embedded disks in U_1
- α_i and β_j meet transversally if they are not disjoint.

It is clear that similar to Heegaard decompositions, a manifold Y admits many different Heegaard diagrams.

Example 2.1. Here is a genus 1 Heegaard decomposition of S^3; think of S^3 as $\mathbb{R}^3 \cup \{\infty\}$, and the Heegaard surface Σ as a torus sitting in $\mathbb{R}^3$. Then, the closure of the bounded component of $\mathbb{R}^3 \setminus \Sigma$ is a handlebody. Call it U_1. Observe that the closure of $S^3 \setminus U_1$ is also a genus 1 handlebody, and here it corresponds to U_0. Then, a choice of the α curve may be a circle on Σ bounding a disk in the unbounded component of $\mathbb{R}^3 \setminus \Sigma$, and a choice of the β curve may be a circle on Σ generating $\frac{H_1(\Sigma,\mathbb{Z})}{[\alpha]}$. See Figure 2.1.

Given a Heegaard diagram $(\Sigma, \boldsymbol{\alpha}, \boldsymbol{\beta})$, we say that $\boldsymbol{\alpha}$ (resp. $\boldsymbol{\beta}$) is a collection of attaching circles for U_0 (resp. U_1). Indeed, this is justified by looking at the properties listed above; curves satisfying these 5 conditions determine uniquely the way U_0 and U_1 are glued together. See the Subsection 2.1.2 below. Therefore, the triplet $(\Sigma, \boldsymbol{\alpha}, \boldsymbol{\beta})$ contains all the information of the Heegaard decomposition of $Y = U_0 \cup_\Sigma U_1$.

In general we will consider Heegaard diagrams with a basepoint z chosen from $\Sigma \setminus (\boldsymbol{\alpha} \cup \boldsymbol{\beta})$. The diagram $(\Sigma, \boldsymbol{\alpha}, \boldsymbol{\beta}, z)$ will be called a *"pointed Heegaard diagram"*, although we

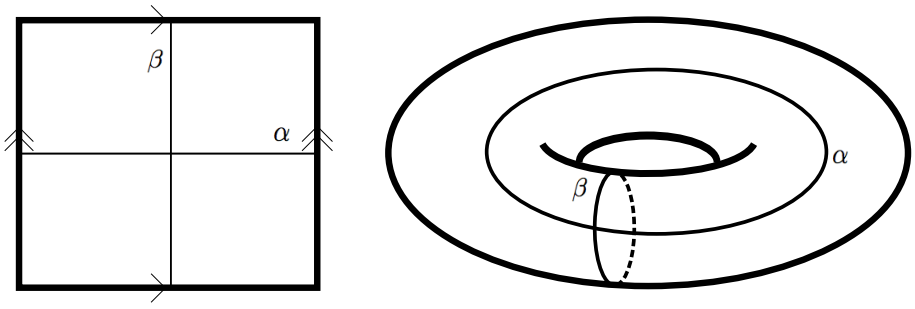

Figure 2.1: A Heegaard diagram for the 3-sphere.

may occasionally refer to it as a Heegaard diagram, given that it will be used much more frequently than diagrams without a basepoint.

It should now be clear that from a given Heegaard diagram, we can recover the handlebodies and consequently, the underlying 3-manifold. What about the converse? Do all closed oriented 3-manifolds admit a Heegaard decomposition?

Proposition 2.1. *Every closed oriented 3-manifold Y admits a Heegaard decomposition.*

Proof. Take any triangulation of the manifold Y. Observe that a triangulation exists since Y is 3-dimensional, closed and orientable. Let F denote the set of vertices and edges of the triangulation. Pick a small regular neighborhood of F. That neighborhood is a handlebody. Call it U_0. $Y \setminus U_0$ is also handlebody, with the same boundary as U_0. □

Another way to prove the proposition above is through Morse theory. See Subsection 2.1.2.

We have already remarked that Y has infinitely many Heegaard diagrams associated to it. Fortunately, we have a way to link all of those Heegaard diagrams together.

Heegaard Moves

There are 3 basic moves on a pointed Heegaard diagram, called "Heegaard moves" that do not change the diffeomorphism class of the underlying manifold. These are the following;

- pointed isotopy

- pointed handle-slide
- stabilization

Pointed isotopy moves the α or the β curves along with the basepoint in a one-parameter family such that the curves remain disjoint from each other and from the basepoint. Handle-slide is an operation of replacing an α_i (or resp. β_i) by a representative of $[\alpha_i]+[\alpha_j]$ (or resp. $[\beta_i] + [\beta_j]$), under the condition that the representative must be a simple closed curve of course. What makes a handle-slide operation "pointed" is that the basepoint in the pointed Heegaard diagram should not lie in the pair of pants bounded by α_i, α_j and the representative of $[\alpha_i] + [\alpha_j]$. The last Heegaard move is the stabilization move, which is basically splicing a 3-sphere to the underlying manifold. Consequently, the obtained manifold is diffeomorphic to the old underlying manifold Y. This happens in terms of Heegaard diagrams in the following way; recall that in Example 2.1, we have given the description of the genus 1 diagram of S^3. Applying stabilization to a diagram $(\Sigma, \alpha_1, \ldots, \alpha_g, \beta_1, \ldots, \beta_g, z)$ yields a new diagram $(\Sigma', \alpha_1, \ldots, \alpha_g, \alpha_{g+1}, \beta_1, \ldots, \beta_g, \beta_{g+1}, z)$, where Σ' is the surface obtained from adjoining a torus to Σ and α_{g+1}, β_{g+1} are exactly as described as in Example 2.1.

Under Heegaard moves, the underlying manifold does not change [16]. Moreover, given two different pointed Heegaard diagrams for the same manifold Y, they can be joined with a finite sequence of Heegaard moves. This will be a fundamental result in the construction of Heegaard Floer homologies.

2.1.2 A Morse theoretic approach

Perhaps a more useful approach to existence of Heegaard diagrams is by using Morse theory.

Let Y be a differentiable manifold and f be a smooth function $f : Y \to \mathbb{R}$. The points on Y where the exterior derivative of f vanishes are called *critical points* of f. If the Hessian matrix (the matrix of second partial derivatives of f) at a critical point P is non-singular, P is called a *non-degenerate critical point* (otherwise it is called a *degenerate critical point*).

Definition. A *Morse function* on a differentiable manifold Y is a smooth function $f : Y \to \mathbb{R}$whose critical points are non-degenerate. The *index of f at the non-degenerate critical point P* is the dimension of the largest subspace of the tangent space at P on which the Hessian matrix at P is negative definite.

Proposition 2.2. (see [9])*(The Morse lemma) Given a Morse function on Y^n and an index i critical point P, there is a diffeomorphism h between a neighborhood W of P and a neighborhood W' of $0 \in \mathbb{R}^n$ such that $h(0) = P$ and*

$$f \circ h(x_1, \ldots, x_n) = -\sum_{j=1}^{i} x_j^2 + \sum_{j=i+1}^{n} x_j^2 + f(P) \tag{2.2}$$

Elementary Morse theory states that if y is a critical value of f with index i, the manifold $f^{-1}(-\infty, y+\epsilon)$ is topologically equivalent to $f^{-1}(-\infty, y-\epsilon)$ with an i-handle attached. A simpler way to state that is, crossing a critical value with index i is equivalent to attaching an i handle to the preimage.

Definition. A Morse function f is said to be "self-indexing", if for every critical point P, the value of the Morse function f at P is equal to the index of f at P.

There exists a self-indexing Morse function f on any 3-manifold Y to [0,3]. See [9] for more background on Morse theory. By the argument above, $f^{-1}[0, 3/2]$ corresponds to a 3-ball with a 1-handle attached for each critical point of f of index 1. That is precisely a handlebody. Observe that $f^{-1}(3/2)$ is the Heegaard surface, and $f^{-1}[3/2, 3]$ is the other handlebody with the same boundary.

It is customary to visualize a Morse function using the classical example of "height function". Referring to the terminology of that example, we can obtain a Heegaard diagram from a self-indexing Morse function and a Riemannian metric on Y as follows;

First, modify the Morse function so that it contains only 1 index 0 and only 1 index 3 point. This can be done if Y is connected, as shown in [9]. Recall that there are as many index 1 critical points as index 2 critical points, and there are exactly g of each, where g is the genus of Σ. Denote the index 1 critical points of f by $P_1, \ldots, P_g$, and index 2 critical points by $Q_1, \ldots, Q_g$. Then, $f^{-1}(3/2)$ is the Heegaard surface, α_i is the set of points in Σ that flow 'down' to P_i (after some rearrangement of the points) with the flow of the vector field $-\nabla f$, and similarly β_j is the set of points in Σ that flow 'up' to Q_j with ∇f. Using Morse lemma, we can show that α_i's and β_j's are simple closed curves. It suffices to prove the claim locally, so assume Q_j is the origin and f is given as in the Morse lemma. Then,

the points (x_1, x_2, x_3) belonging to $f^{-1}(3/2)$ that flow to $0 \in \mathbb{R}^3$ with ∇f satisfy

$$\begin{aligned} \frac{dx_i}{dt} &= -2x_i \quad \text{for } i = 1, 2 \\ \frac{dx_3}{dt} &= 2x_3. \end{aligned}$$

Then, we have

$$\begin{aligned} x_i &= C_i\, e^{-2t} \quad \text{for } i = 1, 2 \\ x_3 &= C_3\, e^{+2t}, \end{aligned}$$

where C_i's are constants and we parametrize such that when $t = 0$, we are at the point P. The constraint of flowing to the origin implies that as t goes to infinity, x_i's go to zero. Hence, we immediately see that $C_3 = 0$. Since x_1, x_2, x_3 has to satisfy $f(x_1, x_2, x_3) = 3/2$ when $t = 0$, we observe that the desired set of points is the solution set for the equation $C_1^2 + C_2^2 = 2 - 3/2$. This is a simple closed curve. Consequently, its diffeomorphic image β_j is a simple closed curve. For the α curves, we proceed in the same manner, except that we solve for the vector field $-\nabla f$.

It is clear that the Heegaard diagram obtained this way is compatible with the Heegaard decomposition induced by the same Morse function.

Let's return for a brief explanation of recovering the 3-manifold Y from a given Heegaard diagram $(\Sigma, \boldsymbol{\alpha}, \boldsymbol{\beta})$. Consider the 3-manifold-with-boundary $\Sigma \times [0, 1]$. Think of the α curves as lying in $\Sigma \times \{0\}$, and the β curves in $\Sigma \times \{1\}$. We will try to complete this object to a closed 3-manifold. It is readily seen that we need to attach two 3-manifolds-with-boundary to $\partial\,(\Sigma \times [0, 1])$, more precisely, one to $\Sigma \times \{0\}$, and another to $\Sigma \times \{1\}$. For the resulting manifold to have no boundary, the attached 3-manifolds-with-boundary must have boundary diffeomorphic to $\Sigma \times \{0\} \cong \Sigma \times \{1\} \cong \Sigma$. Therefore, they are genus g handlebodies, which we denote by U_0 and U_1. It is now a question of how to attach those handlebodies. We know that the α curves must bound disks in U_0 and similarly for the β curves in U_1. After attaching a 2 handle $D^2 \times S^1$ to one of the g α curves, we are reduced to a boundary diffeomorphic to a genus $g - 1$ surface. Repeating this process $g - 1$ more times, we will have boundary diffeomorphic to S^2. Attaching D^2, we get rid of the boundary. Doing the same for $\Sigma \times \{1\}$, we have recovered Y. Observe that the process is well-defined, i.e. the resulting manifold Y is uniquely determined up to diffeomorphism.

2.2 Symmetric Products

From now on, we will work with a given Heegaard diagram $(\Sigma, \boldsymbol{\alpha}, \boldsymbol{\beta}, z)$ of a manifold Y. The g-fold symmetric product of the Heegaard surface Σ is denoted by $Sym^g(\Sigma)$ and defined to be the quotient space of the g-fold Cartesian product of Σ under the action of the symmetric group of g letters S_g. That is, points in $Sym^g(\Sigma)$ are unordered g-tuples of points in Σ. The topology of the symmetric products is studied in [6]. We state here that $Sym^g(\Sigma)$ is a smooth manifold of dimension $2g$ and a complex structure on Σ induces a complex structure on $Sym^g(\Sigma)$ in such a way that the projection map from Σ^g onto $Sym^g(\Sigma)$ is holomorphic. We define the *diagonal* D in $Sym^g(\Sigma)$ to be the g-tuples of points in Σ where the entries are not all distinct.

It was no coincidence that we used the same letter as the genus of Σ when describing the symmetric product. For purposes to be clear later, we consider the g-fold product where g is the genus of Σ. In $Sym^g(\Sigma)$, we have the g-dimensional tori $\mathbb{T}_{\boldsymbol{\alpha}}$ and $\mathbb{T}_{\boldsymbol{\beta}}$, defined to be the quotient of the $(\alpha_1 \times \ldots \times \alpha_g)$ and $(\beta_1 \times \ldots \times \beta_g)$ in the symmetric product. The tori $\mathbb{T}_{\boldsymbol{\alpha}}$ and $\mathbb{T}_{\boldsymbol{\beta}}$ play a critical role in the construction of Heegaard Floer homology, such as yielding the generators of the chain complex. Namely, the generators will be the points in $\mathbb{T}_{\boldsymbol{\alpha}} \cap \mathbb{T}_{\boldsymbol{\beta}}$.

Proposition 2.3. *Let Σ be as above. Then, $\pi_1(Sym^g(\Sigma)) \cong H_1(Sym^g(\Sigma)) \cong H_1(\Sigma)$*

Proof. First, observe that there is a map

$$\begin{aligned} H_1(\Sigma) &\longrightarrow H_1(Sym^g(\Sigma)) \\ [\gamma] &\mapsto [(\gamma, x, \ldots, x)] \end{aligned}$$

where x is a generic point in Σ. It is easy to see that this map is well defined. The inverse mapping can be found in the following way; a closed curve (in general position, i.e. missing the diagonal) in $Sym^g(\Sigma)$ corresponds to a map from a g-fold cover of S^1 to Σ, thus gives a collection of closed curves in Σ. Consequently, each homology class in the symmetric product gives a homology class in $H_1(\Sigma)$. For the well-definedness of this map and the identification $\pi_1(Sym^g(\Sigma)) \cong H_1(Sym^g(\Sigma))$, see [16]

□

Note that any cycle in Y can be deformed into a cycle in Σ. Recall that the curves $\alpha_1, \ldots, \alpha_g, \beta_1, \ldots, \beta_g$ bound disjoint embedded disks in Y. Using the proposition above, we conclude the following.

Corollary. *Let $(\Sigma, \boldsymbol{\alpha}, \boldsymbol{\beta})$ be a Heegaard diagram associated to a manifold Y. Then,*

$$H_1(Y) \cong \frac{H_1(\Sigma)}{[\alpha_1], \ldots, [\alpha_g], [\beta_1], \ldots, [\beta_g]} \cong \frac{H_1(Sym^g(\Sigma))}{H_1(\mathbb{T}_{\boldsymbol{\alpha}}) \oplus H_1(\mathbb{T}_{\boldsymbol{\beta}})} ,$$

where g is the genus of Σ.

The following definition will be useful.

Definition. Let x be a point on Σ. Define $V_x := \{x\} \times Sym^{g-1}(\Sigma)$.

We will generally consider V_z, where z is the basepoint in the given Heegaard diagram. Note that the basepoint is disjoint from $\boldsymbol{\alpha}$ and $\boldsymbol{\beta}$, so $V_z \cap \mathbb{T}_{\boldsymbol{\alpha}} = V_z \cap \mathbb{T}_{\boldsymbol{\beta}} = \emptyset$.

We are going to work with the disks in the symmetric product. To this end, we introduce a notation and present another result concerning the topology of $Sym^g(\Sigma)$. But first, let us define the action of $\pi_1(X)$ on $\pi_n(X)$, where X is a path-connected space.

Let $x \in X$ be any basepoint. Recall that the choice of basepoint is irrelevant since X is path-connected. Let then γ be a loop based at x. We associate, to each continuous mapping $f : (B^n, S^{n-1}) \longrightarrow (X, x)$, another continuous mapping $\gamma \cdot f : (B^n, S^{n-1}) \longrightarrow (X, x)$, obtained by shrinking the domain of f into a smaller disk and completing it to B^n by adjoining γ (with a shrunk domain too) to each radial segment. Then, we set

$$\begin{aligned} \beta_\gamma : \pi_n(X) &\longrightarrow \pi_n(X) \\ [f] &\mapsto [\gamma \cdot f] . \end{aligned}$$

This may be remodeled as follows. We can think of $\gamma \cdot f$ as a map from S^n to X, sending the north pole to x, while at the northern hemisphere, it makes γ along each portion of great circles containing the north pole. Hence, the equator is mapped to x. The southern hemisphere with the equator is diffeomorphic to B^n, and $\gamma \cdot f$ restricted to that ball is the same map as f. We can then identify the equator to get a map from $S^n \vee S^n$. The northern n-sphere can be replaced by a B^1, with one boundary point at the north pole of the northern hemisphere, and the other one at the south pole of the northern hemisphere, which is also the point where B^1 is wedged to the southern n-sphere. And since the boundary points are

mapped to the same point under γ, B^1 may further be replaced by an S^1, taking the free boundary point and identifying with the wedge point, i.e. the north pole of the southern n-sphere. Hence, $\gamma \cdot f$ can also be viewed as a map from $S^1 \vee S^n$ to X. See also Proposition 2.4.

It is easy to check that β_γ is a well-defined group isomorphism, and $\beta_{\gamma_1}\beta_{\gamma_2} = \beta_{\gamma_1\gamma_2}$. Moreover, $[\gamma_1] = [\gamma_2]$ implies $\beta_{\gamma_1} = \beta_{\gamma_2}$. Consequently we get a group homomorphism $\pi_1(X) \to Aut(\pi_n(X))$. That is, each class in the fundamental group of X acts on $\pi_n(X)$.

Let $\pi_2^{'}(X)$ denote the quotient of $\pi_2(X, x)$ under the action of $\pi_1(X, x)$. Note that the quotient group $\pi_2^{'}(X)$ does not depend on the choice of $x \in X$. This is only for dealing with the case where $g = 2$, since when $g > 2$, $\pi_1(Sym^g(\Sigma))$ acts trivially. This is also proved in the next proposition.

Proposition 2.4. *Let Σ be a Riemann surface of genus $g \geq 2$. Then,*

$$\pi_2^{'}(Sym^g(\Sigma)) \cong \mathbb{Z}.$$

Moreover, when $g > 2$, the action of $\pi_1(Sym^g(\Sigma))$ is trivial, hence

$$\pi_2(Sym^g(\Sigma)) \cong \mathbb{Z}.$$

Proof. Let x, $x^{'}$ be distinct generic points in Σ, and τ be an orientation preserving involution of Σ such that $\Sigma/\tau \cong S^2$. Let $S := \left\{(y, \tau(y), x^{'}, \ldots, x^{'}) : y \in \Sigma\right\}$. S is a sphere in $Sym^g(\Sigma)$. S turns out to be the generator of $\pi_2^{'}(Sym^g(\Sigma))$, via the use of the following map counting the algebraic intersection number:

$$\begin{aligned} \varphi : \pi_2^{'}(Sym^g(\Sigma)) &\longrightarrow \mathbb{Z} \\ \phi &\mapsto \#\{\phi \cap V_x\} \end{aligned}$$

This map is invariant under homotopy, which can be seen by intersecting the homotopy with the subvariety $\{x\} \times Sym^{g-1}(\Sigma)$. The intersection will consist of 1-manifolds-with-boundary (since the homotopy is 3 dimensional and the subvariety is $2g-2$ dimensional), and the boundaries of the 1-manifolds (which correspond to the intersection of the homotopic disks with the subvariety) will cancel out to give zero. Since one of the homotopic disks is then counted with the reverse orientation, the intersection numbers of the two disks with

the subvariety must then be the same. Furthermore, given a loop in the symmetric product, the generic intersection number with V_x is zero. Thus, the map above is also invariant under the action of the fundamental group. Therefore, the map φ is well-defined.

It is clear that $\varphi(S) = 1$, since $(x, \tau(x), x', \ldots, x')$ and $(\tau(x), \tau^2(x), x', \ldots, x')$ are the same points in the symmetric product. So, given $n \in \mathbb{Z}$, $\varphi(nS) = n$, where nS is obtained by splicing S to $(n-1)S$ for $n \geq 2$, and $-nS$ is nS with the reverse orientation. Note that the splicing here does not specify any basepoints, so it takes place in $\pi_2'(Sym^g(\Sigma))$.

We will now separate the cases $g = 2$ and $g > 2$. First, let $g > 2$ and θ be a sphere in the kernel of φ. Then, if θ misses $\{x\} \times Sym^{g-1}(\Sigma)$ already, we can say that $\theta \in Sym^g(\Sigma \setminus \{x\})$. If not, then moving θ in general position, we can assure that θ meets $\{x\} \times Sym^{g-1}(\Sigma)$ in finitely many points. We want to obtain a sphere homotopic to θ but missing the diagonal. For that, we splice homotopic translates of S with appropriate signs to θ at those points. Namely, if at some point $(x, x_2, \ldots, x_g) \in V_x$, θ intersects V_x positively (resp. negatively), we splice $-S$ (resp. S) to θ at that point. The algebraic count of intersections is zero, therefore total number of S spliced to θ is equal to that of $-S$. Since $S*(-S)$ is homotopically trivial. The new sphere obtained represents the same homotopy class as θ and is disjoint from V_x. Therefore, it lies in $Sym^g(\Sigma \setminus \{x\})$. It only remains to see that $\pi_2(Sym^g(\Sigma \setminus \{x\})) = 0$. Note that $\Sigma \setminus \{x\}$ is homotopically equivalent to $\mathbb{C} \setminus \{z_1, \ldots, z_{2g}\}$ where z_i are distinct points. Then, $Sym^g(\Sigma \setminus \{x\})$ is homotopically equivalent to $Sym^g(\mathbb{C} \setminus \{z_1, \ldots, z_{2g}\})$, and $Sym^g(\mathbb{C} \setminus \{z_1, \ldots, z_{2g}\})$ can be seen as the space of monic degree g polynomials p in one variable, with $p(z_i) \neq 0$ for all $i \in \{1, \ldots, 2g\}$, via the map

$$(a_1, \ldots, a_g) \mapsto (x - a_1) \cdot \ldots \cdot (x - a_g).$$

This is nothing but $\mathbb{C}^g$ minus $2g$ generic hyperplanes. A theorem of Hattori states that the homology groups of the universal covering space of this complement are trivial except in dimension 0 or g [16]. The claim follows. In the case where $g = 2$, $Sym^g(\Sigma)$ is diffeomorphic to the blowup of T^4 [16]. Then, the claim in the proposition holds.

Finally, we prove that the action of $\pi_1(Sym^g(\Sigma))$ is trivial for $g > 3$. Let $(x, \ldots, x)$ be a generic point in the symmetric product. Let

$$\gamma : S^1 \longrightarrow Sym^g(\Sigma)$$
$$\sigma : S^2 \longrightarrow Sym^g(\Sigma)$$

be given maps based around $(x, \dots, x)$. We want to prove that the map

$$\gamma \vee \sigma : S^1 \vee S^2 :\longrightarrow Sym^g(\Sigma)$$

is homotopic to the map

$$c_{(x,\dots,x)} \vee \sigma : S^1 \vee S^2 :\longrightarrow Sym^g(\Sigma),$$

where S^1 and S^2 are wedged at a point which is mapped to $(x, \dots, x) \in Sym^g(\Sigma)$, and $C_{(x,\dots,x)}$ is the constant loop. By Proposition 2.3, we can replace γ by a homotopic curve in the form $(\gamma_1, x, \dots, x)$ for some $\gamma_1 : S^1 \longrightarrow \Sigma$. Similarly, since $\pi_2'(Sym^g(\Sigma)) \cong \mathbb{Z}$, by choosing x as a fixed point of the involution when creating the generator S, we can find a map $\sigma_1 : S^2 \longrightarrow Sym^g(\Sigma)$ such that σ is homotopic to (σ_1, x) for some $\sigma_1 : S^2 \longrightarrow Sym^{g-1}(\Sigma)$. Therefore, we get a map

$$\gamma_1 \times \sigma_1 : S^1 \times S^2 \longrightarrow Sym^g(\Sigma),$$

and the composition $S^1 \vee S^2 \longrightarrow S^1 \times S^2 \longrightarrow Sym^g(\Sigma)$ is equal to $\gamma \vee \sigma$, where the first arrow is the map taking $t \in S^1$ to (t, w_2), and $z \in S^2$ to (w_1, z), with w_i's being the points at which the 1 and 2-spheres are wedged. Observe that $\gamma_1(w_1) = \sigma_1(w_2) = (x, \dots, x)$.

But the action of $\pi_1(S^1 \times S^2)$ on $\pi_2(S^1 \times S^2)$ is trivial, so the first map in the above composition is homotopic to $\{w_1\} \vee \imath$, which takes all $t \in S^1$ to (w_1, w_2), and $z \in S^2$ to (w_1, z). Consequently, they are still homotopic when composed with $\gamma_1 \times \sigma_1$, and this is exactly what we wanted to prove. □

We close this subsection by mentioning a structural property of $\mathbb{T}_{\boldsymbol{\alpha}}$ and $\mathbb{T}_{\boldsymbol{\beta}}$.

Definition. Let Z be a complex manifold and J a complex structure on it. A submanifold $L \subseteq Z$ is called *totally real* if for all $\lambda \in L$, $T_\lambda L \cap JT_\lambda L = \{0\}$, i.e. if the tangent spaces of L does not contain a J-complex line.

Proposition 2.5. *Let $(\Sigma, \boldsymbol{\alpha}, \boldsymbol{\beta})$ be a Heegaard diagram. Then, $\mathbb{T}_{\boldsymbol{\alpha}}$ and $\mathbb{T}_{\boldsymbol{\beta}}$ are totally real in $Sym^g(\Sigma)$.*

Proof. It is easy to see that $\mathbb{T}_{\boldsymbol{\alpha}}$ and $\mathbb{T}_{\boldsymbol{\beta}}$ are totally real in Σ^g with respect to the product complex structure. Since the α_j's are disjoint, the tori $\mathbb{T}_{\boldsymbol{\alpha}}$ and $\mathbb{T}_{\boldsymbol{\beta}}$ miss the diagonal D. Therefore, the inverse image of some neighborhood of $\mathbb{T}_{\boldsymbol{\alpha}}$ consists of disjoint copies of this

tori, and it restricts to a diffeomorphism at one of these copies. Similar for $\mathbb{T}_{\boldsymbol{\beta}}$. The claim follows. □

2.2.1 Intersection points and disks in symmetric products

The aim of this subsection will be to prove Proposition 2.6. For that, we now introduce some definitions, after which the reader is advised to glance at Proposition 2.6 on page 17 for motivation.

Let $\mathbf{x}, \mathbf{y} \in \mathbb{T}_{\boldsymbol{\alpha}} \cap \mathbb{T}_{\boldsymbol{\beta}}$ be two intersection points. Let $a : [0,1] \longrightarrow \mathbb{T}_{\boldsymbol{\alpha}}$, $b : [0,1] \longrightarrow \mathbb{T}_{\boldsymbol{\beta}}$ be two paths from $\mathbf{x}$ to $\mathbf{y}$ in $\mathbb{T}_{\boldsymbol{\alpha}}$ and $\mathbb{T}_{\boldsymbol{\beta}}$ respectively. Note that $a - b$ is a loop in $Sym^g(\Sigma)$.

Definition. Let $\epsilon(\mathbf{x}, \mathbf{y})$ denote the image of $a - b$ in $H_1(Y, \mathbb{Z})$ under the map presented in the corollary to Proposition 2.3.

If $a^{'}$, $b^{'}$ are other paths from $\mathbf{x}$ to $\mathbf{y}$ in $\mathbb{T}_{\boldsymbol{\alpha}}$ and $\mathbb{T}_{\boldsymbol{\beta}}$ respectively, then

$$(a - b) - (a^{'} - b^{'}) = (a - a^{'}) - (b - b^{'}),$$

and $(a - a^{'})$ and $(b - b^{'})$ are loops in $\mathbb{T}_{\boldsymbol{\alpha}}$ and $\mathbb{T}_{\boldsymbol{\beta}}$ respectively, which are killed when working in $H_1(Y, \mathbb{Z})$. Therefore, $\epsilon(\mathbf{x}, \mathbf{y})$ is independent from the choice of the paths a, b. This immediately implies that ϵ is additive, i.e. if $\mathbf{z}$ is another point of intersection, then

$$\epsilon(\mathbf{x}, \mathbf{z}) = \epsilon(\mathbf{x}, \mathbf{y}) + \epsilon(\mathbf{y}, \mathbf{z})$$

Let $\mathbb{D}$ denote the unit disk in $\mathbb{C}$. Let ρ_r denote the arc $\partial\mathbb{D} \cap \{z \in \mathbb{C}; Re(z) \geq 0\}$, and ρ_l denote $\partial\mathbb{D} \cap \{z \in \mathbb{C}; Re(z) \leq 0\}$.

Definition. Let $\mathbf{x}$, $\mathbf{y}$ be a pair of intersection points. A *Whitney disk connecting* $\mathbf{x}$ *to* $\mathbf{y}$ is defined to be a continuous map

$$\phi : \mathbb{D} \longrightarrow Sym^g(\Sigma)$$

satisfying the following:

- $\phi(i) = \mathbf{x}$, $\phi(-i) = \mathbf{y}$
- $\phi(\rho_l) \subset \mathbb{T}_{\boldsymbol{\alpha}}$, $\phi(\rho_r) \subset \mathbb{T}_{\boldsymbol{\beta}}$,

We also define $\pi_2(\mathbf{x}, \mathbf{y})$ to be the set of homotopy classes of Whitney disks connecting $\mathbf{x}$ and $\mathbf{y}$.

The set $\pi_2(\mathbf{x}, \mathbf{y})$ is endowed with a multiplication;

$$\pi_2^{'}(Sym^g(\Sigma)) * \pi_2(\mathbf{x}, \mathbf{y}) \longrightarrow \pi_2(\mathbf{x}, \mathbf{y})$$

which splices the sphere nS to ϕ in order to get a new Whitney disk connecting $\mathbf{x}$ to $\mathbf{y}$. Furthermore, if $\mathbf{z}$ is another point of intersection, we have another multiplicative operation

$$\begin{aligned} * : \pi_2(\mathbf{x}, \mathbf{y}) \times \pi_2(\mathbf{y}, \mathbf{z}) &\longrightarrow \pi_2(\mathbf{x}, \mathbf{z}) \\ (\phi_1, \phi_2) &\mapsto \phi_3 \end{aligned}$$

where ϕ_3 is the disk obtained by gluing ϕ_1 to ϕ_2 at $\mathbf{y}$.

We remark that if there is a Whitney disk ϕ connecting $\mathbf{x}$ to $\mathbf{y}$, then $\epsilon(\mathbf{x}, \mathbf{y}) = 0$, since the boundary of that disk (which is homologically trivial of course) maps to $\epsilon(\mathbf{x}, \mathbf{y})$ under the homomorphism in the definition of $\epsilon(\mathbf{x}, \mathbf{y})$. Therefore, we can introduce the following equivalence class; We define the equivalence relation $\sim$ on $\mathbb{T}_{\boldsymbol{\alpha}} \cap \mathbb{T}_{\boldsymbol{\beta}}$, where we declare two points $\mathbf{x}$ and $\mathbf{y}$ to be equivalent iff $\epsilon(\mathbf{x}, \mathbf{y}) = 0$. Note that transitivity of $\sim$ follows from the additivity of ϵ.

Domains

We will now in some sense "project" the disks in the symmetric product to the Heegaard surface. Let $\mathbf{x}, \mathbf{y} \in \mathbb{T}_{\boldsymbol{\alpha}} \cap \mathbb{T}_{\boldsymbol{\beta}}$. In Proposition 2.4), we used a function giving the algebraic intersection number of the spheres with the subvarieties determined by a basepoint. The following additive assignment does the same for Whitney disks.

Definition. Pick $w \in \Sigma \setminus \boldsymbol{\alpha} \cup \boldsymbol{\beta}$. Let

$$\begin{aligned} n_w : \pi_2(\mathbf{x}, \mathbf{y}) &\longrightarrow \mathbb{Z} \\ \phi &\mapsto \#\{\phi \cap V_w\} \end{aligned}$$

be the map giving the algebraic intersection number of the disk ϕ and the submanifold V_w

For instance, ϕ and V_w are intersecting $+1$ (-1 resp.) at a point $(w, x_2, \ldots, x_g)$ if their orientation add up to give the canonical orientation (opposite orientation resp.) of $Sym^g(\Sigma)$.

To justify the claim we have made that n_w is additive, observe that $\phi_1 * \phi_2$ intersects V_w exactly at the points of intersection of ϕ_1 and V_w and the points of intersection of ϕ_2 and V_w. That is because we splice the two disks together to obtain $\phi_1 * \phi_2$. This assignment has also another property for the sphere splicing operation; observe that $\#\{S \cap V_w\} = 1$ for any point w, so we have

$$n_w(S * \phi) = 1 + n_w(\phi).$$

Definition. Let $D_1, \ldots, D_m$ denote the closures of the connected components of $\Sigma \setminus (\alpha_1 \cup \ldots \cup \alpha_g \cup \beta_1 \cup \ldots \cup \beta_g)$. For any $\phi \in \pi_2(\mathbf{x}, \mathbf{y})$, we define the *domain associated to* ϕ to be the formal sum

$$D(\phi) = \sum_{i=1}^{m} n_{z_i}(\phi) D_i \,,$$

where z_i is a generic point of interior of D_i for any $i \in \{1, \ldots, m\}$.

Recall that the boundary of ϕ is on $\mathbb{T}_{\boldsymbol{\alpha}} \cup \mathbb{T}_{\boldsymbol{\beta}}$, so the domain associated to ϕ does not depend on the choice of points z_i. We write $D(\phi) \geq 0$ if all the coefficients $n_{z_i}(\phi)$ in the formal sum are nonnegative.

The results that n_w is additive and $n_w(S) = 1$ imply immediately the following.

$$D(\phi_1 * \phi_2) = D(\phi_1) + D(\phi_2) \tag{2.3}$$

$$D(S * \phi) = D(\phi) + \sum_{i=1}^{m} D_i \tag{2.4}$$

Now, let's see what happens in terms of the boundaries of the domains. Let $\mathbf{x} = (x_1, \ldots, x_g)$, $\mathbf{y} = (y_1, \ldots, y_g)$ be two points of intersection, where

$$x_i \in \alpha_i \cap \beta_i$$

$$y_i \in \alpha_i \cap \beta_{\sigma(i)}$$

for all i, with σ being a permutation in S_m. Note that we have not specified anything upto this point, since, the conditions above can be obtained by a simple re-indexing of the coordinates of $\mathbf{x}$ and $\mathbf{y}$. If $\phi \in \pi_2(\mathbf{x}, \mathbf{y})$, recall the notations in the definition of a Whitney disk, and observe that $\phi(i) = \mathbf{x}$, $\phi(-i) = \mathbf{y}$, and $\phi(\rho_l) \subset \mathbb{T}_{\boldsymbol{\alpha}}$, $\phi(\rho_r) \subset \mathbb{T}_{\boldsymbol{\beta}}$ imply that the restriction of $\phi(\rho_l)$ to α_i starts from x_i and ends at y_i. Similar for β_i, with the exception that it starts at $y_{\sigma(i)}$ and ends at x_i. Therefore, we have established the following.

1. $\partial D(\phi)|_{\alpha_i}$ is a 1-chain with boundary $y_i - x_i$.

2. $\partial D(\phi)|_{\beta_i}$ is a 1-chain with boundary $x_i - y_{\sigma(i)}$.

We say that a formal sum $A = \sum_{i=1}^{m} a_i D_i$ connects $\mathbf{x}$ to $\mathbf{y}$ if ∂A connects $\mathbf{x}$ to $\mathbf{y}$ along the α curves and $\mathbf{y}$ to $\mathbf{x}$ along the β curves. The properties above state that $D(\phi)$ connects $\mathbf{x}$ to $\mathbf{y}$.

Finally, we have arrived at the following.

Proposition 2.6. *Assume $g \geq 3$, let $\mathbf{x}$, $\mathbf{y}$ be two intersection points. Then, $\epsilon(\mathbf{x}, \mathbf{y}) \neq 0$ implies $\pi_2(\mathbf{x}, \mathbf{y}) = \emptyset$, otherwise,*

$$\pi_2(\mathbf{x}, \mathbf{y}) \cong \mathbb{Z} \oplus H^1(Y, \mathbb{Z})$$

When $g = 2$, we have the same result except that $\epsilon(\mathbf{x}, \mathbf{y}) = 0$ implies

$$\pi_2'(\mathbf{x}, \mathbf{y}) \cong \mathbb{Z} \oplus H^1(Y, \mathbb{Z}),$$

where $\pi_2'(\mathbf{x}, \mathbf{y})$ can be constructed by modding out $\pi_2(\mathbf{x}, \mathbf{y})$ with the relation: ϕ_1 is equivalent to ϕ_2 iff $D(\phi_1) = D(\phi_2)$.

Proof. Let $\Omega(Sym^g(\Sigma))$ be the space of paths in $Sym^g(\Sigma)$ with fixed endpoints, and $\Omega(\mathbb{T}_{\boldsymbol{\alpha}}, \mathbb{T}_{\boldsymbol{\beta}})$ be the subspace consisting of paths connecting $\mathbb{T}_{\boldsymbol{\alpha}}$ to $\mathbb{T}_{\boldsymbol{\beta}}$. Note that the space $\pi_2(\mathbf{x}, \mathbf{x})$ is naturally identified with the fundamental group of the space $\Omega(\mathbb{T}_{\boldsymbol{\alpha}}, \mathbb{T}_{\boldsymbol{\beta}})$ based at $(\mathbf{x})$, the constant path at the point $\mathbf{x}$.

There is a natural evaluation map from $\Omega(\mathbb{T}_{\boldsymbol{\alpha}}, \mathbb{T}_{\boldsymbol{\beta}})$ to $\mathbb{T}_{\boldsymbol{\alpha}} \times \mathbb{T}_{\boldsymbol{\beta}}$, sending the path to its endpoints. This map induces a fibration with fiber space $\Omega(Sym^g(\Sigma))$.

$$\Omega(Sym^g(\Sigma)) \longrightarrow \Omega(\mathbb{T}_{\boldsymbol{\alpha}}, \mathbb{T}_{\boldsymbol{\beta}}) \longrightarrow \mathbb{T}_{\boldsymbol{\alpha}} \times \mathbb{T}_{\boldsymbol{\beta}}$$

Looking at part of the associated homotopy long exact sequence, we obtain;

$$\pi_2(\mathbb{T}_{\boldsymbol{\alpha}} \times \mathbb{T}_{\boldsymbol{\beta}}) \longrightarrow \pi_1(\Omega(Sym^g(\Sigma))) \longrightarrow \pi_1(\Omega(\mathbb{T}_{\boldsymbol{\alpha}}, \mathbb{T}_{\boldsymbol{\beta}})) \longrightarrow \pi_1(\mathbb{T}_{\boldsymbol{\alpha}} \times \mathbb{T}_{\boldsymbol{\beta}}) \longrightarrow \pi_0(\Omega(Sym^g(\Sigma))).$$

Observe that $\pi_1(\Omega(Sym^g(\Sigma)))$ is the space of loops of paths based at the constant path $\mathbf{x}$, and the symmetric product is path connected, so this space is isomorphic to $\pi_2(Sym^g(\Sigma))$,

with the notation of Proposition 2.4. Additionally, we already have the three identifications below.

$$\begin{aligned}\pi_2(\mathbb{T}_{\boldsymbol{\alpha}} \times \mathbb{T}_{\boldsymbol{\beta}}) &\cong \pi_2(\mathbb{T}_{\boldsymbol{\alpha}}) \oplus \pi_2(\mathbb{T}_{\boldsymbol{\beta}}) \cong 0 \\ \pi_1(\mathbb{T}_{\boldsymbol{\alpha}} \times \mathbb{T}_{\boldsymbol{\beta}}) &\cong \pi_1(\mathbb{T}_{\boldsymbol{\alpha}}) \oplus \pi_1(\mathbb{T}_{\boldsymbol{\beta}}) \\ \pi_1(\Omega(\mathbb{T}_{\boldsymbol{\alpha}}, \mathbb{T}_{\boldsymbol{\beta}})) &\cong \pi_2(\mathbf{x}, \mathbf{x})\end{aligned}$$

Hence, the exact sequence above becomes;

$$0 \longrightarrow \pi_2(Sym^g(\Sigma)) \longrightarrow \pi_2(\mathbf{x}, \mathbf{x}) \longrightarrow \pi_1(\mathbb{T}_{\boldsymbol{\alpha}}) \oplus \pi_1(\mathbb{T}_{\boldsymbol{\beta}}) \longrightarrow \pi_1(Sym^g(\Sigma))$$

Suppose now $g > 2$. Recall, by Proposition 2.4, we have $\pi_2(Sym^g(\Sigma) \cong \mathbb{Z}$. Moreover, by Proposition 2.3, the fundamental group $\pi_1(Sym^g(\Sigma))$ is equal to the first homology group, which in turn is isomorphic to first cohomology group $H^1(\Sigma)$ by Poincaré duality. Under that identification, $\pi_1(\mathbb{T}_{\boldsymbol{\alpha}})$ and $\pi_1(\mathbb{T}_{\boldsymbol{\beta}})$ correspond to $H^1(U_0)$ and $H^1(U_1)$ respectively. Hence, we have

$$0 \longrightarrow \mathbb{Z} \longrightarrow \pi_2(\mathbf{x}, \mathbf{x}) \longrightarrow H^1(U_0) \oplus H^1(U_1) \longrightarrow H^1(\Sigma).$$

It now remains to see that the kernel of the map $H^1(U_0) \oplus H^1(U_1) \longrightarrow H^1(\Sigma)$ is isomorphic to $H^1(Y)$. But this map is the direct sum of the maps induced by the inclusions

$$\begin{aligned}\Sigma &\longrightarrow U_0 \\ \Sigma &\longrightarrow U_1.\end{aligned}$$

Considering also the inclusions of U_0 and U_1 in Y, we obtain a cohomology exact sequence

$$H^0(U_0) \oplus H^0(U_1) \longrightarrow H^0(\Sigma) \longrightarrow H^1(Y) \longrightarrow H^1(U_0) \oplus H^1(U_1) \longrightarrow H^1(\Sigma)$$

The map on the very left is easily seen to be onto, therefore $H^1(Y)$ injects onto the kernel of the required map.

When $g = 2$, the proof is the same, but we need to mod out the action of $\pi_1(Sym^g(\Sigma))$[16][11].

For the general case, whenever we have $\pi_2(\mathbf{x}, \mathbf{y}) \neq \emptyset$, $\epsilon(\mathbf{x}, \mathbf{y}) = 0$, i.e. it bounds a disk D in the symmetric product. Then, we have a map from $\pi_2(\mathbf{x}, \mathbf{x})$ to $\pi_2(\mathbf{x}, \mathbf{y})$which concatenates the disk D, and another map from $\pi_2(\mathbf{x}, \mathbf{y})$ to $\pi_2(\mathbf{x}, \mathbf{x})$ splicing $-D$, where $-D$ is the disk obtained by rotating the plane by an angle of π. It is easy to see that these maps are inverses of each other, so the two groups are isomorphic. □

Here, the summand $\mathbb{Z}$ corresponds to the subset "generated" by the sphere S, and the summand $H^1(Y,\mathbb{Z})$ is related to the homology classes of 2-cycles in Y by the Poincaré duality.

Moreover, when $g \geq 2$, we have the following;

Proposition 2.7. [11] *Let $g \geq 2$. Suppose A is a domain connecting $\mathbf{x}$ to $\mathbf{y}$. Then, there is a homotopy class $\phi \in \pi_2(\mathbf{x},\mathbf{y})$ such that $D(\phi) = A$. Furthermore, ϕ is uniquely determined by A when $g > 2$.*

Therefore, homotopy classes $\pi_2(\mathbf{x},\mathbf{y})$ are in 1-1 correspondence with domains connecting $\mathbf{x}$ to $\mathbf{y}$.

2.3 Spin^c Structures

In this section, we will attempt to derive a *Spin^c* structure from each point of intersection in $\mathbb{T}_{\boldsymbol{\alpha}} \cap \mathbb{T}_{\boldsymbol{\alpha}}$. For this, let's first introduce the concept of a *Spin^c* structure.

There are various ways to define a *Spin^c* structure, among which we will use the reformulation for 3-manifolds due to Turaev.

Our ambient manifold Y is three dimensional, so it has Euler characteristic zero, therefore Y admits nowhere vanishing vector fields. Let v_1, v_2 be two such vector fields.

Definition. We say that v_1 is *homologous* to v_2 if there is a ball B such that $v_1|_{Y\setminus B}$ is homotopic to $v_2|_{Y\setminus B}$.

"Being homologous to" is a transitive relation, because given two balls, we can always find a bigger one containing both of these balls, and transitivity of homotopy is carried on to the desired transitivity outside the big ball.

Definition. We define the *Spin^c structures over Y* to be the set of nowhere vanishing vector fields over Y modulo the equivalence relation above. We denote this set by *Spin^c*(Y).

Given a Heegaard diagram $(\Sigma, \boldsymbol{\alpha}, \boldsymbol{\beta}, z)$, we can now introduce the method to obtain a *Spin^c* structure from an intersection point. Namely, we define here a map

$$s_z : \mathbb{T}_{\boldsymbol{\alpha}} \cap \mathbb{T}_{\boldsymbol{\beta}} \longrightarrow Spin^c(Y)$$

in the following way.

Take a self indexing Morse function f compatible with the diagram $(\Sigma, \boldsymbol{\alpha}, \boldsymbol{\beta}, z)$, with only 1 index zero and only 1 index three point. Recall the discussion about the Morse theoretic approach to Heegaard diagrams. For convenience, we re-state here that a point $x \in \Sigma$ in the intersection of α_i and β_j flows from an index 1 point P_i to an index 2 point Q_j with ∇f. Then, any $\mathbf{x} = (x_1, \ldots, x_g)$ specifies a g-tuple of trajectories flowing from distinct index 1 points to distinct index 2 points. Similarly, since $z \notin \alpha \cup \beta$, it specifies a trajectory connecting the index 0 point to the index 3 point. Then, delete tubular neighborhoods of these $g+1$ trajectories. Observe that in the boundaries of these tubular neighborhoods, the vector field ∇f has index zero because they all contain two singular points of different parities. It follows that the vector field can be extended to a new non-vanishing vector field over Y. Define $s_z(\mathbf{x})$ to be the homology class of this nowhere vanishing vector field. Observe that $s_z(\mathbf{x})$ is uniquely determined because we can find a ball B containing all the tubular neighborhoods we have deleted and re-filled, so any two extensions of ∇f are homotopic.

It is proved in [16] that $s_z(\mathbf{x}) - s_z(\mathbf{y}) = PD\,[\epsilon(\mathbf{x}, \mathbf{y})]$.

2.4 Holomorphic disks and the Maslov index

Recall that a complex structure on Σ induces a complex structure on $Sym^g(\Sigma)$. Given a homotopy class $\phi \in \pi_2(\mathbf{x}, \mathbf{y})$, define $\mathcal{M}(\phi)$ to be the moduli space of holomorphic representatives of ϕ. One uses appropriate perturbations described in [3], [4], [5] in order to prove that $\mathcal{M}(\phi)$ is a smooth manifold.

We will make use of an $\mathbb{R}$-action on $\mathcal{M}(\phi)$ described as follows: Using Riemann Mapping theorem, map the unit disk $\mathbb{D}$ to the infinite strip $[0,1] \times i\mathbb{R} \subset \mathbb{C}$, such that ρ_l is transformed to $\{0\} \times i\mathbb{R}$ and ρ_r is transformed to $\{1\} \times i\mathbb{R}$. Then, $r \in \mathbb{R}$ acts as a vertical translation by r. It is the action of the group of complex automorphisms preserving i and $-i$ [11]. We will divide $\mathcal{M}(\phi)$ by that action to get the unparametrized moduli space:

$$\widehat{\mathcal{M}(\phi)} = \frac{\mathcal{M}(\phi)}{\mathbb{R}}$$

By definition, the $\mathbb{R}$ action above is free, except the case where ϕ is constant, i.e. $\phi \in \pi_2(\mathbf{x}, \mathbf{x})$ with $D(\phi) = 0$. In that case, $\mathcal{M}(\phi)$ is a singleton corresponding to the constant map.

We will count holomorphic disks in the unparametrized moduli space $\widehat{\mathcal{M}(\phi)}$. For that

to be significant, or non-trivial one might say, we will be interested in the cases where the moduli space $\mathcal{M}(\phi)$ is 1-dimensional, so that when we mod out the $\mathbb{R}$ action, we get a zero dimensional manifold, i.e. a signed collection of points. The signs are induced by the orientations. It is proved in [16] that there is a natural choice of orientations for all moduli spaces which is coherent.

The moduli space $\mathcal{M}(\phi)$ has an expected dimension called the *Maslov index*, denoted by $\mu(\phi)$. See [18] for details. The Maslov index is additive, i.e.

$$\mu(\phi_1 * \phi_2) = \mu(\phi_1) + \mu(\phi_2)$$

and it is zero for the homotopy class of the constant disk. Furthermore, it satisfies the following.

Proposition 2.8. [11] *Let $\phi \in \pi_2(\mathbf{x}, \mathbf{y})$, then the Maslov index satisfies*

$$\mu(kS * \phi) = \mu(\phi) + 2k$$

Using properties of holomorphic disks, we establish,

Proposition 2.9. *Let $\phi \in \pi_2(\mathbf{x}, \mathbf{y})$, then $\mathcal{M}(\phi) \neq \emptyset$ implies that $D(\phi) \geq 0$.*

Proof. Pick a generic point z_i in each D_i. Since V_{z_i} is a submanifold with the induced complex structure, the holomorphic disk ϕ must meet it with correct orientation, given that it does meet it. □

The next result is proved in [16].

Theorem 2.1. *There is a family of perturbations with the property that if $\mu(\phi) = 1$ then $\widehat{\mathcal{M}(\phi)}$ is a compact zero dimensional manifold.*

2.5 Chain Complexes and Homology Groups

We will define the Heegaard Floer homology groups for the cases where Y is a rational homology sphere, i.e. the rational homology groups of Y are the same as the three sphere S^3. This will be sufficient in order to proceed to knot and link invariants in the next chapter. Let Y be a rational homology sphere, $(\Sigma, \boldsymbol{\alpha}, \boldsymbol{\beta}, z)$ be a genus g Heegaard diagram, and t be a $Spin^c$ structure over Y.

2.5.1 $\widehat{HF}(Y,t)$

Let $\widehat{CF}(\Sigma,\boldsymbol{\alpha},\boldsymbol{\beta},t)$ denote the free $\mathbb{Z}$-module generated by the intersection points $\mathbf{x}\in\mathbb{T}_{\boldsymbol{\alpha}}\cap\mathbb{T}_{\boldsymbol{\beta}}$ such that $s_z(\mathbf{x})=t$. We define a relative grading called the *Maslov grading* on the generators as follows:

$$gr(\mathbf{x},\mathbf{y})=\mu(\phi)-2n_z(\phi),$$

where ϕ is any homotopy class in $\pi_2(\mathbf{x},\mathbf{y})$.

On the other hand, a relative grading is by definition additive, which in this case follows easily from the additivity of the Maslov index and the function n_z. To see that this relative grading is independent of the choice of the homotopy class, recall propositions 2.6 and 2.8. Since Y is a rational homology sphere, $H^1(Y,\mathbb{Z})=0$, therefore $\pi_2(\mathbf{x},\mathbf{y})\cong\mathbb{Z}$. So, any other choice of homotopy class would be of the form $kS*\phi$, and the result follows.

Definition. Given a homotopy class $\phi\in\pi_2(\mathbf{x},\mathbf{y})$, we define $c(\phi)$ to be the signed number of points in $\widehat{\mathcal{M}(\phi)}$. If $\mu(\phi)$ is different from 1, we declare $c(\phi)$ to be zero.

We remark that the definition above makes sense in view of Theorem 2.1. Second part of the definition is just a convention in order to ignore unparametrized holomorphic disks with bigger or no dimension in the definition of the differential operator below. This count geometrically is a signed count of points in a compact oriented 0-dimensional manifold.

We endow $\widehat{CF}(\Sigma,\boldsymbol{\alpha},\boldsymbol{\beta},t)$ with the following differential map which is extended linearly:

$$\begin{array}{rcccl}\partial:\widehat{CF}(\Sigma,\boldsymbol{\alpha},\boldsymbol{\beta},t) & \longrightarrow & \widehat{CF}(\Sigma,\boldsymbol{\alpha},\boldsymbol{\beta},t) & & \\ \mathbf{x} & \mapsto & \partial\mathbf{x} = & \displaystyle\sum_{\left\{\substack{\mathbf{y}\in\mathbb{T}_\alpha\cap\mathbb{T}_\beta \\ \phi\in\pi_2(\mathbf{x},\mathbf{y})}\ |\ n_z(\phi)=0\right\}} & c(\phi)\cdot\mathbf{y}\end{array}$$

First of all, note that we always encounter finite formal sums since there is a unique homotopy class ϕ satisfying $n_z(\phi)=0$ since $<S>=\pi_2(\mathbf{x},\mathbf{y})\cong\mathbb{Z}$. Moreover, the count in the definition of the map ∂ does not exceed $\widehat{CF}(\Sigma,\boldsymbol{\alpha},\boldsymbol{\beta},t)$, since the existence of a disk connecting $\mathbf{x}$ to $\mathbf{w}$ implies $s_z(\mathbf{w})=s_z(\mathbf{x})=t$.

Of course, we need to justify that the map defined above is a differential, i.e. $\partial^2=0$. The next theorem establishes that and contains arguments that will be referred later.

Theorem 2.2. *The pair* $\left(\widehat{CF}(\Sigma,\boldsymbol{\alpha},\boldsymbol{\beta},t),\ \partial\right)$ *is a chain complex.*

Proof. First of all, applying the map ∂ twice, we obtain the following.

$$\partial^2\mathbf{x} = \sum_{\left\{\begin{smallmatrix}\mathbf{w},\mathbf{y}\in\mathbb{T}_\alpha\cap\mathbb{T}_\beta\\ \phi\in\pi_2(\mathbf{x},\mathbf{w})\end{smallmatrix}\right\}} \sum_{\left\{\begin{smallmatrix}\phi_1\in\pi_2(\mathbf{x},\mathbf{y}) & n_z(\phi_1)=0\\ \phi_2\in\pi_2(\mathbf{y},\mathbf{w}) \mid & n_z(\phi_2)=0\\ & \phi_1*\phi_2=\phi\end{smallmatrix}\right\}} c(\phi_1)c(\phi_2)\cdot\mathbf{w}$$

$\mu(\phi)\neq 1$ implies that $c(\phi)=0$, therefore the generators $\mathbf{y}$ appearing in the expression of $\partial\mathbf{x}$ all satisfy $gr(\mathbf{x},\mathbf{y})=1$, since we only count classes ϕ with $n_z(\phi)=0$. Therefore, using this argument twice, we conclude that the generators $\mathbf{w}$ appearing in the expression of $\partial^2(\mathbf{x})$ are in relative grading -2 with respect to $\mathbf{x}$. That is,

$$gr(\mathbf{x},\mathbf{w})=\mu(\mathbf{x},\mathbf{w})=2.$$

Therefore, For any fixed $\phi\in\pi_2(\mathbf{x},\mathbf{w})$, $\widehat{\mathcal{M}(\phi)}$ is 1-dimensional. Hence, we will analyze the "ends" of the compactification of the moduli space $\widehat{\mathcal{M}(\phi)}$. By Floer theory, this space has 3 kinds of ends;

1. "broken flow-lines", i.e. a concatenation of two classes $\phi_1\in\pi_2(\mathbf{x},\mathbf{y})$, $\phi_2\in\pi_2(\mathbf{y},\mathbf{w})$ with $\mu(\phi_1)=\mu(\phi_2)=1$.

2. those which correspond to a sphere "bubbling off", i.e. a $\phi\in\pi_2(\mathbf{x},\mathbf{w})$ and a holomorphic sphere Θ in the symmetric product that meets ϕ.

3. those which correspond to "boundary bubbling", i.e. a $\phi\in\pi_2(\mathbf{x},\mathbf{w})$ and a holomorphic map u from the disk whose boundary is mapped into $\mathbb{T}_{\boldsymbol{\alpha}}$ or $\mathbb{T}_{\boldsymbol{\beta}}$, which meet in a point on that boundary.

We will see that "bubbling off" and "boundary bubbling" cannot occur in our case. First, By Proposition 2.9, a holomorphic sphere satisfying $n_z(\phi)=0$ can be considered as lying in $Sym^g(\Sigma\setminus\{z\})$. Therefore, we only count disks in $Sym^g(\Sigma\setminus\{z\})$ when applying the differential map above. But in view of an argument used in the proof of Proposition 2.4, there are no nontrivial spheres in $Sym^g(\Sigma\setminus\{z\})$. Therefore "bubbling off" of a sphere is ruled out. Also, a disk u with boundary lying in $\mathbb{T}_{\boldsymbol{\alpha}}$ or in $\mathbb{T}_{\boldsymbol{\beta}}$ will admit a domain $D(u)$ greater than or equal to Σ [16] (the boundary of the domain will be in the α curves, but $\Sigma\setminus\boldsymbol{\alpha}$ is connected). This similarly is not the case since a degeneration of our type of disks cannot intersect V_z. Hence, only boundary components are the broken flow-lines. That is,

the boundary of the compactification of $\widehat{\mathcal{M}(\phi)}$, which is a 1-dimensional compact manifold (therefore has zero dimensional boundary, i.e. isolated points with signs, whose algebraic count is zero), consist of all the broken flow-lines disjoint from V_z, and nothing else (since if there is a flow between two points of intersection, they produce the same $Spin^c$ structure via the method given in 2.3). That is, for any ϕ flowing from $\mathbf{x}$ to $\mathbf{w}$, we have

$$\sum_{\left\{\begin{smallmatrix}\mathbf{y}\in\mathbb{T}_\alpha\cap\mathbb{T}_\beta\\ \phi_1\in\pi_2(\mathbf{x},\mathbf{y})\\ \phi_2\in\pi_2(\mathbf{y},\mathbf{w})\end{smallmatrix} \mid \begin{smallmatrix} n_z(\phi_1)=n_z(\phi_2)=0\\ \phi_1*\phi_2=\phi\end{smallmatrix}\right\}} c(\phi_1)c(\phi_2)\cdot\mathbf{w} \;=0$$

Then, summing over all possible flows from $\mathbf{x}$ to $\mathbf{w}$, we get

$$\sum_{\mathbf{y}\in\mathbb{T}_\alpha\cap\mathbb{T}_\beta}\sum_{\left\{\begin{smallmatrix}\phi_1\in\pi_2(\mathbf{x},\mathbf{y})\\ \phi_2\in\pi_2(\mathbf{y},\mathbf{w})\end{smallmatrix} \mid \begin{smallmatrix} n_z(\phi_1)=0\\ n_z(\phi_2)=0\end{smallmatrix}\right\}} c(\phi_1)c(\phi_2)\cdot\mathbf{w} \;=0$$

Finally, to include all the terms in the expression of $\partial^2(\mathbf{x})$, summing over all intersection points in $\widehat{CF}(\Sigma,\boldsymbol{\alpha},\boldsymbol{\beta},t)$ gives the desired result;

$$\partial^2\mathbf{x} \;=\sum_{\left\{\begin{smallmatrix}\mathbf{w}\,,\mathbf{y}\,\in\mathbb{T}_\alpha\cap\mathbb{T}_\beta\\ \phi\in\pi_2(\mathbf{x},\mathbf{w})\end{smallmatrix}\right\}}\sum_{\left\{\begin{smallmatrix}\phi_1\in\pi_2(\mathbf{x},\mathbf{y})\\ \phi_2\in\pi_2(\mathbf{y},\mathbf{w})\end{smallmatrix} \mid \begin{smallmatrix} n_z(\phi_1)=0\\ n_z(\phi_2)=0\\ \phi_1*\phi_2=\phi\end{smallmatrix}\right\}} c(\phi_1)c(\phi_2)\cdot\mathbf{w} \;=0$$

□

Definition. The Heegaard Floer homology groups $\widehat{HF}(\Sigma,\boldsymbol{\alpha},\boldsymbol{\beta},t)$ are the homology groups of the chain complex $\Big(\widehat{CF}(\Sigma,\boldsymbol{\alpha},\boldsymbol{\beta},t),\,\partial\Big)$.

It is proved in [16] that the Heegaard Floer homology constructed this way remains invariant under the Heegaard moves explained in the paragraph 2.1.1. More explicitly, an other choice of any of the constructions used in the definition such as the Heegaard diagram, complex structure, etc., yields a chain homotopy equivalent complex. Recall that any two different pointed Heegaard diagrams for the same manifold Y can be joined with a finite sequence of Heegaard moves. Hence, we have the following theorem:

Theorem 2.3. *Let Y be a closed orientable 3-manifold, $(\Sigma,\boldsymbol{\alpha},\boldsymbol{\beta},z)$, $(\Sigma',\boldsymbol{\alpha}',\boldsymbol{\beta}',z')$ be two Heegaard diagrams of Y, $t\in Spin^c(Y)$ be a $Spin^c$ structure over Y. Then, the Heegaard Floer homology groups $\widehat{HF}(\Sigma,\boldsymbol{\alpha},\boldsymbol{\beta},t)$ and $\widehat{HF}(\Sigma,\boldsymbol{\alpha}',\boldsymbol{\beta}',t)$ are isomorphic.*

Therefore, we are allowed to drop out Σ, $\boldsymbol{\alpha}$, $\boldsymbol{\beta}$ in the expression of the Heegaard Floer homology groups and write $\widehat{HF}(Y,t)$ instead of $\widehat{HF}(\Sigma,\boldsymbol{\alpha},\boldsymbol{\beta},t)$.

2.5.2 $HF^\infty(Y,t)$, $HF^-(Y,t)$, $HF^+(Y,t)$

Recall that when defining $\widehat{HF}(Y,t)$, we only took into account the holomorphic disks disjoint from the subvariety V_z determined by the basepoint $z \in \Sigma$. On the other hand, another construction without this preliminary elimination is possible. However, the basepoint z will still play a role.

Let U be an indeterminate over $\mathbb{Z}$. Now, in contrast with the previous subsection, we will define $CF^\infty(\Sigma, \boldsymbol{\alpha}, \boldsymbol{\beta}, t)$ to be the free $\mathbb{Z}(U)$-module generated by the intersection points $\mathbf{x} \in \mathbb{T}_{\boldsymbol{\alpha}} \cap \mathbb{T}_{\boldsymbol{\beta}}$ with $s_z(\mathbf{x}) = t$. We will give the generators the same Maslov grading as before, and add the condition that multiplication by U drops the grading by two. That is, we extend the previous grading as follows;

$$gr(U^i \mathbf{x}, U^j \mathbf{y}) = gr(\mathbf{x}, \mathbf{y}) + 2(j - i)$$

We introduce the differential map ∂^∞ on generators below. Note that this map is extended linearly, so we have $\partial^\infty (U^i \mathbf{x}) = U^i \partial^\infty \mathbf{x}$.

$$\begin{aligned} \partial^\infty : CF^\infty(\Sigma, \boldsymbol{\alpha}, \boldsymbol{\beta}, t) &\longrightarrow CF^\infty(\Sigma, \boldsymbol{\alpha}, \boldsymbol{\beta}, t) \\ \mathbf{x} &\mapsto \partial^\infty \mathbf{x} = \sum_{\left\{\substack{\mathbf{y} \in \mathbb{T}_\alpha \cap \mathbb{T}_\beta \\ \phi \in \pi_2(\mathbf{x}, \mathbf{y})}\right\}} c(\phi) \cdot U^{n_z(\phi)} \mathbf{y} \end{aligned}$$

Observe that the sum is again finite, since, similar to the previous subsection, if $\mu(\phi) \neq 1$, $c(\phi)$ vanishes, and there is only one homotopy class $\phi \in \pi_2(\mathbf{x}, \mathbf{y})$ satisfying $\mu(\phi) = 1$. Moreover, if $U^j \mathbf{y}$ appears in $\partial^\infty \mathbf{x}$, we have $j = n_z(\phi)$ for some $\phi \in \pi_2(\mathbf{x}, \mathbf{y})$, and then

$$gr(\mathbf{x}, U^j \mathbf{y}) = \mu(\phi) - 2n_z(\phi) + 2j = \mu(\phi) = 1$$

so each term in $\partial^\infty \mathbf{x}$ is in relative Maslov grading -1 with respect to $\mathbf{x}$.

The proof for $\partial^\infty \circ \partial^\infty = 0$ is similar to Theorem 2.2 but requires further technical detail, so we skip it here.

Definition. Let $CF^-(\Sigma, \boldsymbol{\alpha}, \boldsymbol{\beta}, t)$ be the subgroup of $CF^\infty(\Sigma, \boldsymbol{\alpha}, \boldsymbol{\beta}, t)$ generated by the same intersection points as before, but over $\mathbb{Z}[U]$. Define $CF^+(\Sigma, \boldsymbol{\alpha}, \boldsymbol{\beta}, t)$ to be the quotient group

$$CF^\infty(\Sigma, \boldsymbol{\alpha}, \boldsymbol{\beta}, t) / CF^-(\Sigma, \boldsymbol{\alpha}, \boldsymbol{\beta}, t)$$

We will denote the induced differential maps by ∂^- and ∂^+ respectively.

In view of Proposition 2.9 and assuming that $CF^\infty(\Sigma, \boldsymbol{\alpha}, \boldsymbol{\beta}, t)$ is a chain complex we prove the next result;

Proposition 2.10. *The subgroup $CF^-(\Sigma, \boldsymbol{\alpha}, \boldsymbol{\beta}, t)$ is a subcomplex of $CF^\infty(\Sigma, \boldsymbol{\alpha}, \boldsymbol{\beta}, t)$. Moreover, the sequence*

$$0 \to CF^-(\Sigma, \boldsymbol{\alpha}, \boldsymbol{\beta}, t) \longrightarrow CF^\infty(\Sigma, \boldsymbol{\alpha}, \boldsymbol{\beta}, t) \longrightarrow CF^+(\Sigma, \boldsymbol{\alpha}, \boldsymbol{\beta}, t) \to 0$$

of chain complexes, where the first map is inclusion and the second is projection, is exact.

Proof. The related result on the boundary maps of $CF^-(\Sigma, \boldsymbol{\alpha}, \boldsymbol{\beta}, t)$ and $CF^+(\Sigma, \boldsymbol{\alpha}, \boldsymbol{\beta}, t)$ follows from the skipped fact that $\partial^\infty \circ \partial^\infty = 0$. We only need to see that $CF^-(\Sigma, \boldsymbol{\alpha}, \boldsymbol{\beta}, t)$ is closed under the differential map $\partial^- = \partial^\infty$.

Assume $U^j \mathbf{y}$ appears in $\partial^\infty(U^i \mathbf{x})$. Then, there is a homotopy class $\phi \in \pi_2(\mathbf{x}, \mathbf{y})$ with $c(\phi) \neq 0$, such that $n_z(\phi) = j - i$. Moreover, by Proposition 2.9, $n_z(\phi) \geq 0$. Therefore,

$$U^i \mathbf{x} \in CF^-(\Sigma, \boldsymbol{\alpha}, \boldsymbol{\beta}, t) \iff i \geq 0 \implies j \geq 0 \iff U^j \mathbf{y} \in CF^-(\Sigma, \boldsymbol{\alpha}, \boldsymbol{\beta}, t)$$

so $CF^-(\Sigma, \boldsymbol{\alpha}, \boldsymbol{\beta}, t)$ is a chain complex.

The exactness of the sequence is trivial. □

Definition. The Heegaard Floer homology groups $HF^\infty(\Sigma, \boldsymbol{\alpha}, \boldsymbol{\beta}, t), HF^+(\Sigma, \boldsymbol{\alpha}, \boldsymbol{\beta}, t), HF^-(\Sigma, \boldsymbol{\alpha}, \boldsymbol{\beta}, t)$ are defined to be the homology groups of $CF^\infty(\Sigma, \boldsymbol{\alpha}, \boldsymbol{\beta}, t), CF^+(\Sigma, \boldsymbol{\alpha}, \boldsymbol{\beta}, t), CF^-(\Sigma, \boldsymbol{\alpha}, \boldsymbol{\beta}, t)$ respectively.

It is proved in [15] that for rational homology spheres, $HF^\infty(\Sigma, \boldsymbol{\alpha}, \boldsymbol{\beta}, t)$ is always isomorphic to $\mathbb{Z}(U)$. We also have an invariance result as in the previous case of $\widehat{HF}$, proved in [16], allowing to drop Σ, $\boldsymbol{\alpha}$, $\boldsymbol{\beta}$ from the notation and define

$$HF^+(Y, t) = HF^+(\Sigma, \boldsymbol{\alpha}, \boldsymbol{\beta}, t)$$
$$HF^-(Y, t) = HF^-(\Sigma, \boldsymbol{\alpha}, \boldsymbol{\beta}, t).$$

2.5.3 Heegaard Floer Homologies when $b_1(Y) \neq 0$

We have constructed several homology groups for rational homology spheres. These manifolds Y satisfy $b_1(Y) = 0$, and consequently we obtained $\pi_2(\mathbf{x}, \mathbf{y}) \cong \mathbb{Z}$ in view of Proposition

2.6. For manifolds with nonzero $b_1(Y)$, $\pi_2(\mathbf{x}, \mathbf{y})$ is larger. The arising difficulties in this case is solved using special Heegaard diagrams. The only difference is the Floer homologies may not admit relative grading [11].

Chapter 3

KNOT FLOER AND LINK FLOER HOMOLOGIES

The homologies constructed in the previous chapter can be extended to obtain knot or link invariants for knots or links in closed oriented three manifolds via use of extra basepoints on the Heegaard surface. In this chapter, we will establish the adaptation of these invariants, which will also include an alternate way to define the same homologies. More details on this subject can be found on [11], [8].

3.1 Knot Floer Homology

A knot in S^3 is an oriented embedding of S^1 into S^3. It is by definition a 1-dimensional closed submanifold of S^3. Two knots are said to be *"isotopic"* if there exists a continuous transformation between them.

Recall the discussion in Section 2.3. In the definition of the function s_z, where $z \in \Sigma$ is a basepoint, using a compatible Morse function, we described a way to obtain a flow connecting the index 0 point to the index 3 point. Therefore, if we consider the Heegaard diagrams $(\Sigma, \boldsymbol{\alpha}, \boldsymbol{\beta}, z, w)$ with an additional base point w, we get two such flows. Then, it is obvious that these two flows piece together to form a knot in Y.

Knot Floer homology deals with knots in 3-manifolds, but we will only work in S^3 in order to simplify the discussion. Let $(\Sigma, \boldsymbol{\alpha}, \boldsymbol{\beta}, z, w)$ be a 2-pointed Heegaard diagram for S^3. Another way to obtain a knot using the basepoints w, z is as follows. Let a be a path joining w and z in $\Sigma \setminus \boldsymbol{\alpha}$, and b be another path connecting the basepoints in $\Sigma \setminus \boldsymbol{\beta}$. Push a and b into U_0 and U_1, respectively. The result is a knot K in S^3, which is isotopic to the one explained in the previous paragraph. We say that the 2-pointed diagram $(\Sigma, \boldsymbol{\alpha}, \boldsymbol{\beta}, z, w)$ is compatible with the knot K.

Note that we will not mention $Spin^c$ structures when defining Knot Floer homology. It is proved in [11] that $Spin^c(Y)$ is in one-to-one correspondence with $H^2(Y, \mathbb{Z})$. Therefore, $H^2(S^3, \mathbb{Z}) = 0$ implies that there is a unique $Spin^c$ structure on S^3.

Using Morse theory, one can show that every knot in S^3 has a compatible 2-pointed Heegaard diagram. Namely, let f be a self-indexing Morse function on K with only two critical points, one index 0 and one index 3. Then, extend f to a self-indexing function $\tilde{f}$ on S^3 in such a way that the index 1 and index 2 critical points of $\tilde{f}$ are disjoint from K. Consider the Heegaard diagram induced by $\tilde{f}$. Let the basepoints be the two intersection points of K with $\tilde{f}^{-1}(3/2)$. Note that there are no more than two intersection points since then we would obtain another critical point of f.

3.1.1 $\widehat{HFK}(K)$

Let $(\Sigma, \boldsymbol{\alpha}, \boldsymbol{\beta}, z, w)$ be a Heegaard diagram compatible with the knot K, and let $C_K(\Sigma, \boldsymbol{\alpha}, \boldsymbol{\beta}, z, w)$ be the free $\mathbb{Z}$-module generated by the intersection points $\mathbf{x} \in \mathbb{T}_\alpha \cap \mathbb{T}_\beta$. An immediate adaptation of the Heegaard Floer homology group $\widehat{HF}(Y,t)$ is the following.

Consider the map

$$\begin{aligned} \partial_K : C_K(\Sigma, \boldsymbol{\alpha}, \boldsymbol{\beta}, z, w) &\longrightarrow C_K(\Sigma, \boldsymbol{\alpha}, \boldsymbol{\beta}, z, w) \\ \mathbf{x} &\mapsto \sum_{\left\{ \begin{smallmatrix} \mathbf{y} \in \mathbb{T}_\alpha \cap \mathbb{T}_\beta \\ \phi \in \pi_2(\mathbf{x},\mathbf{y}) \end{smallmatrix} \mid \begin{smallmatrix} \mu(\phi)=1 \\ n_z(\phi)=n_w(\phi)=0 \end{smallmatrix} \right\}} c(\phi) \cdot \mathbf{y}, \end{aligned}$$

where $c(\phi)$ is as defined in Section 2.5.

Observe that we merely apply the natural use of the extra basepoint here, i.e. we only count holomorphic disks disjoint from the subvarieties V_w as well as V_z.

Proposition 3.1. $\partial_K \circ \partial_K = 0$

Proof. Recall the proof of Theorem 2.2. The 1-dimensional moduli space $\widehat{\mathcal{M}(\phi)}$, where $\phi \in \pi_2(\mathbf{x}, \mathbf{z})$, has 3 kinds of ends, "broken flow-lines", "boundary bubbles", "bubbling offs". By the same argument in the proof, there are no "bubbling off" of a sphere, nor there are "boundary bubbles". Hence, we only encounter broken flow-lines. Since a compact 1-dimensional manifold has zero dimensional boundary with algebraic count zero, we have

$$0 = \sum_{\left\{ \begin{smallmatrix} \phi_1 \in \pi_2(\mathbf{x},\mathbf{y}) \\ \phi_2 \in \pi_2(\mathbf{y},\mathbf{z}) \end{smallmatrix} \mid \begin{smallmatrix} n_z(\phi_1)=n_z(\phi_2)=0 \\ n_w(\phi_1)=n_w(\phi_2)=0 \\ \phi_1 * \phi_2 = \phi \end{smallmatrix} \right\}} c(\phi_1)c(\phi_2) \cdot \mathbf{z}$$

Summing over all possible flows from $\mathbf{x}$ to $\mathbf{z}$, and then summing over all intersection points $\mathbf{z}$, we obtain the desired result. □

Consequently, the pair $(C_K(\Sigma, \boldsymbol{\alpha}, \boldsymbol{\beta}, z, w), \partial_K)$ is a chain complex. It is also true that the induced homology is invariant under Heegaard moves. Consequently, it is independent from the Heegaard diagram representing K.

Definition. Let $\widehat{HFK}(K)$ denote the homology of the chain complex $(C_K(\Sigma, \boldsymbol{\alpha}, \boldsymbol{\beta}, z, w), \partial_K)$.

We introduce here a bigrading on the generators of $C_K(\Sigma, \boldsymbol{\alpha}, \boldsymbol{\beta}, z, w)$, both relative.

Let $\mathbf{x}$ and $\mathbf{y}$ be two intersection points and let ϕ be a holomorphic disk in $\pi_2(\mathbf{x}, \mathbf{y})$.

Definition. We define the relative Alexander grading by

$$A(\mathbf{x}, \mathbf{y}) = n_z(\phi) - n_w(\phi).$$

We also have a natural extension of the Maslov grading in $\widehat{CF}$.

Definition. We provide the generators of $C_K(\Sigma, \boldsymbol{\alpha}, \boldsymbol{\beta}, z, w)$ with another relative grading, called the Maslov grading, by

$$gr(\mathbf{x}, \mathbf{y}) = \mu(\phi) - 2n_w(\phi).$$

We observe at once that these gradings are independent of the choice of the homotopy class, in virtue of the Propositions 2.6 and 2.8.

It should be remarked here that a generator appearing in $\partial_K(\mathbf{x})$ is in relative Maslov grading -1 with respect to $\mathbf{x}$. On the other hand, it is in the same Alexander grading. From this point of view, the Alexander grading does not seem to help matters, but it will come into play once we will start counting holomorphic disks intersecting V_z or V_w.

Another remark would be in the roles of the basepoints z and w in these gradings. It is clear that interchanging z and w, we get the same knot with the reverse orientation. In this case, there is no problem there since we only count holomorphic disks that are disjoint from both V_z and V_w.

Similarly, we can mimic the construction of the homology groups CF^∞, CF^+ and CF^- to obtain analogues for the knots. However, we will only make room for $HFK^-(K)$, the adaptation of HF^-, since the recipe for the other groups can be easily derived from the data already present.

3.1.2 $HFK^-(K)$

This subsection presents a direct way to define the homolog group $HFK^-(K)$. The idea is easily applicable to the previous chapter.

Let $(\Sigma, \boldsymbol{\alpha}, \boldsymbol{\beta}, z, w)$ be a Heegaard diagram for the knot K. This time, let $C_K^-(\Sigma, \boldsymbol{\alpha}, \boldsymbol{\beta}, z, w)$, the free $\mathbb{Z}[U]$-module generated by all the intersection points, where U is an indeterminate. We will introduce a new differential map, and modify the relative gradings accordingly.

As before, this is to put the disks intersecting V_w into play. For doing so, we have to keep track of the intersection numbers by the use of the indeterminate U. On the other hand, we will force the intersection number of V_z with the holomorphic disks that we count to be zero, for the vanishing of the square of the differential map.

We introduce the differential map ∂^-:

$$\begin{aligned} \partial^- : C_K^-(\Sigma, \boldsymbol{\alpha}, \boldsymbol{\beta}, z, w) &\longrightarrow C_K^-(\Sigma, \boldsymbol{\alpha}, \boldsymbol{\beta}, z, w) \\ \mathbf{x} &\mapsto \sum_{\left\{ \substack{\mathbf{y} \in \mathbb{T}_\alpha \cap \mathbb{T}_\beta \\ \phi \in \pi_2(\mathbf{x},\mathbf{y})} \,\middle|\, \substack{\mu(\phi)=1 \\ n_z(\phi)=0} \right\}} c(\phi) \cdot U^{\,n_w(\phi)}\, \mathbf{y} \,. \end{aligned}$$

Next, we extend the Maslov grading on the generators of $C_K^-(\Sigma, \boldsymbol{\alpha}, \boldsymbol{\beta}, z, w)$ with the formula below;

$$gr(U^i\,\mathbf{x}, U^j\,\mathbf{y}) = gr(\mathbf{x}, \mathbf{y}) + 2(j - i)$$

Consequently, whenever a term $U^j\,\mathbf{y}$ appears in $\partial^-\mathbf{x}$, we have $j = n_w(\phi)$ for some $\phi \in \pi_2(\mathbf{x}, \mathbf{y})$, and then

$$gr(\mathbf{x}, U^j\,\mathbf{y}) = \mu(\phi) - 2n_w(\phi) + 2j = \mu(\phi) = 1$$

so all the terms appearing in the differential of $\mathbf{x}$ are in relative Maslov grading -1 with respect to $\mathbf{x}$.

In similarity with the extension above, the relative Alexander grading is now given by the formula below.

$$A(U^i\,\mathbf{x}, U^j\,\mathbf{y}) = A(\mathbf{x}, \mathbf{y}) + (j - i)$$

Therefore, if $U^j\,\mathbf{y}$ appears in $\partial^-(U^i\,\mathbf{x})$, keeping in mind that there exists a holomorphic disk flowing from $\mathbf{x}$ to $\mathbf{y}$ with the property $n_w(\phi) = j - i$, we have

$$A(U^i\,\mathbf{x}, U^j\,\mathbf{y}) = n_z(\phi) - n_w(\phi) + j - i = n_w(\phi) + j - i = 0$$

One may also affirm equivalently that the indeterminate U drops Maslov grading by 2, while it drops Alexander grading by 1.

Definition. We define $HFK^-(K)$ to be the homology of the chain complex $\left(C_K^-(\Sigma, \boldsymbol{\alpha}, \boldsymbol{\beta}, z, w), \partial^-\right)$, which is independent of the Heegaard diagram compatible with K.

It is possible to advance one step further with these ideas in order to obtain link invariants. This is the subject of the next section.

3.2 Link Floer Homology

A link in S^3 is a 1-dimensional closed submanifold of the 3-sphere whose connected components are knots. We say that L is an "l-component link" if the number of connected components of the link L is equal to l.

Recall that two distinct basepoints in the Heegaard surface Σ yield a knot in S^3. The idea here is to allow more basepoints, partitioned into groups of 2, where each group gives a knot in S^3. Then, for instance, if $z_1, w_1, \ldots, z_l, w_l$ are $2g$ distinct points on $\Sigma \setminus (\boldsymbol{\alpha} \cup \boldsymbol{\beta})$, we get an l-component link in S^3 following the same method in the previous section. The result concerning the existence of a Heegaard diagram for an arbitrary knot K is also valid for links.

Let now $(\Sigma, \boldsymbol{\alpha}, \boldsymbol{\beta}, z_1, w_1, \ldots, z_l, w_l)$ be a Heegaard diagram for an l-component link L. For convenience, let $\mathcal{Z}$ and $\mathcal{W}$ denote the set of basepoints $z_1, \ldots, z_l$ and $w_1, \ldots, w_l$ respectively. The adaptation of the concepts of the previous section is then almost straightforward. However, we will now proceed in a slightly different way, first establishing the group $HFL^-(L)$ and then acquiring $\widehat{HFL}(L)$. Even so, the only significant modification will be the one concerning the Alexander grading. In fact, it will be a "filtration" (see the definition below) instead of being a grading.

Let $U_1, \ldots, U_n$ be indeterminates over the ring $\mathbb{Z}$. Consider the partial ordering "$\preceq$" on $\mathbb{Z}^l$, where $(a_1, \ldots, a_l) \preceq (b_1, \ldots, b_l)$ if for all $i = 1, \ldots, l$ we have $a_i \leq b_i$. We remark here that $(a_1, \ldots, a_l) \prec (b_1, \ldots, b_l)$ iff $(a_1, \ldots, a_l) \preceq (b_1, \ldots, b_l)$ and for some i, $a_i \neq b_i$. For the sake of simplicity, let n be a positive integer, g be a function $g : \{1, \ldots, n\} \to \mathbb{Z}^l$ such that $(0, \ldots, 0) \preceq g(i)$ for all $i \in \{1, \ldots, n\}$.

Definition. A $\mathbb{Z}^l$ filtration on a $\mathbb{Z}[U_1,\dots,U_n]$-module M is a collection of $\mathbb{Z}[U_1,\dots,U_n]$-submodules $\{\mathcal{F}_s(M)\}_{s\in\mathbb{Z}^l}$ satisfying the properties:

- $\mathcal{F}_s(M)\subseteq\mathcal{F}_t(M)$ if $s\preceq t$
- there exists $s\in\mathbb{Z}^l$ such that $\mathcal{F}_s(M)=M$.
- $U^i\mathcal{F}_s(M)\subseteq\mathcal{F}_{s-g(i)}(M)$

Moreover, we define *"the filtration level"* of $x\in M$ to be $s\in\mathbb{Z}^l$ such that $x\in\mathcal{F}_s(M)$ and $x\notin\mathcal{F}_t(M)$ whenever $t\prec s$.

Definition. We say that a chain complex C is *"filtered"* if there is a filtration on C.

The additional data n is digressive for now (we will set n to be equal to l), though it will be necessary in the next chapter. We had to introduce numerous technical details for a relatively easy concept, but we are ready to start now.

Let $C_L^-(\Sigma,\boldsymbol{\alpha},\boldsymbol{\beta},\mathcal{Z},\mathcal{W})$ be the free $\mathbb{Z}[U_1,\dots,U_l]$-module generated by the intersection points. The differential map ∂^- is given by:

$$\begin{aligned}\partial^- : C_L^-(\Sigma,\boldsymbol{\alpha},\boldsymbol{\beta},\mathcal{Z},\mathcal{W}) &\longrightarrow C_L^-(\Sigma,\boldsymbol{\alpha},\boldsymbol{\beta},\mathcal{Z},\mathcal{W})\\ \mathbf{x} &\mapsto \sum_{\left\{\substack{\mathbf{y}\in\mathbb{T}_\alpha\cap\mathbb{T}_\beta\\ \phi\in\pi_2(\mathbf{x},\mathbf{y})}\ \middle|\ \substack{\mu(\phi)=1\\ n_{z_1}(\phi)=\dots=n_{z_l}(\phi)=0}\right\}} c(\phi)\cdot U_1^{n_{w_1}(\phi)}\cdots U_l^{n_{w_l}(\phi)}\mathbf{y}\end{aligned}$$

In terms of the Maslov grading, we have a straightforward extension;

$$\begin{aligned} gr(\mathbf{x},\mathbf{y}) &= \mu(\phi)-2\sum_{i=1}^{l} n_{w_i}(\phi)\\ gr(U_1^{i_1}\cdots U_l^{i_l}\cdot\mathbf{x},U_1^{j_1}\cdots U_l^{j_l}\cdot\mathbf{y}) &= gr(\mathbf{x},\mathbf{y})+2(j_1+\ldots+j_l)-2(i_1+\ldots+i_l)\end{aligned}$$

Again, all the terms appearing in $\partial^-\mathbf{x}$ are in relative Maslov grading -1 with respect to $\mathbf{x}$.

Finally, the Alexander grading of Knot Floer homology now becomes the Alexander filtration on $C_L^-(\Sigma,\boldsymbol{\alpha},\boldsymbol{\beta},\mathcal{Z},\mathcal{W})$. We set $g:\{1,\dots,l\}\to\mathbb{Z}^l$, where $g(i)$ is the i^{th} standard basis vector in $\mathbb{Z}^l$.

Definition. For $s = (s_1, \ldots, s_l) \in \mathbb{Z}^l$, we define $\mathcal{F}_s(C_L^-(\Sigma, \boldsymbol{\alpha}, \boldsymbol{\beta}, \mathcal{Z}, \mathcal{W}))$ to be the submodule generated over $\mathbb{Z}$ by the points $U_1^{a_1} \cdots U_l^{a_l} \cdot \mathbf{x}$ where $(-a_1, \ldots, -a_l) \preceq (s_1, \ldots, s_l)$. Moreover, we set that multiplication by U_i drops the filtration level by $g(i)$, i.e. the i^{th} term of the filtration level is dropped by 1. Finally, we define $A : C_L^-(\Sigma, \boldsymbol{\alpha}, \boldsymbol{\beta}, \mathcal{Z}, \mathcal{W}) \to \mathbb{Z}^l$ to be the function giving the filtration level.

It is elementary to check that the Alexander filtration defined above is a filtration. A simplified but equivalent way to re-describe the Alexander filtration may be to assert that, for every $\mathbf{x}, \mathbf{y} \in \mathbb{T}_{\boldsymbol{\alpha}} \cap \mathbb{T}_{\boldsymbol{\beta}}$,

1. $A(\mathbf{x}) - A(\mathbf{y}) = (n_{z_1}(\phi) - n_{w_1}(\phi)\,, \ \ldots\ , \ n_{z_l}(\phi) - n_{w_l}(\phi))$ where ϕ flows from $\mathbf{x}$ to $\mathbf{y}$

2. $A\left(U_1^{a_1} \cdots U_l^{a_l} \cdot \mathbf{x}\right) = A(\mathbf{x}) - \sum_{i=1}^{l} a_i \cdot g(i)$

We define $HFL^-(L)$ to be the homology of the chain complex $\left(C_L^-(\Sigma, \boldsymbol{\alpha}, \boldsymbol{\beta}), \partial^-\right)$.

Definition. The *associated graded object* of a filtered chain complex is defined as the chain complex

$$gr(C) = \bigoplus_{s \in \mathbb{Z}^l} gr_s(C),$$

where $gr_s(C)$ is the quotient module of $\mathcal{F}_s(C)$ by the submodule generated by $\mathcal{F}_t(C)$ for all $t \prec s$. Moreover, $gr_s(C)$ is endowed with the differential induced from the differential map in C.

We may recuperate $\widehat{HFL}(L)$, which only counts holomorphic disks disjoint from each of the subvarieties determined by the basepoints, merely by setting $U_1 = \cdots = U_l = 0$ in $C_L^-(\Sigma, \boldsymbol{\alpha}, \boldsymbol{\beta})$ and taking the associated graded object. It is easy to see that we have the same generators as in the other way of construction, and the differential map is also the same since $U_i = 0$ for all i implies we only count disks disjoint from all the basepoints.

It is not difficult to check that link Floer homology becomes knot Floer homology when $l = 1$, i.e. when the link L is in fact a knot.

3.3 Link Floer Homology with Multiple Basepoints

In the process of establishing Heegaard Floer homology and the knot and link invariants of the previous sections, we needed the α curves that constitute $\boldsymbol{\alpha}$ to span half of the first homology group of the Heegaard surface, as well as the β curves (recall that there are as many α (or β) curves as the genus of Σ and we required those curves to be homologically linearly independent). But then, the same span may also be acquired with more curves, some of them homologically redundant. Of course, if that is the case, the extra α and β curves would lead us to an augmented number of intersection points, and consequently to a seemingly more complicated way to compute Heegaard Floer homology. In Chapter 4, we will see that this method can have its own advantages, such as yielding an easy to understand, nevertheless computationally expensive algorithm. Note that this formulation require the coefficients to come from the field $\mathbb{F}_2 = \mathbb{Z}/2\mathbb{Z}$.

The result is the so-called "combinatorial link Floer homology", studied in the next chapter. From that viewpoint, introducing multiple basepoints is just an auxiliary step, mainly for establishing the connection between combinatorial and classical link Floer homology.

3.3.1 Multiple Pointed Surface

Let k be a positive integer. Suppose we are given a genus g Heegaard surface Σ, two sets of pairwise disjoint simple closed curves $\boldsymbol{\alpha} = \{\alpha_1, \ldots, \alpha_{g+k-1}\}$, $\boldsymbol{\beta} = \{\beta_1, \ldots, \beta_{g+k-1}\}$ such that they both span a g dimensional subspace of the first homology group $H_1(\Sigma)$ which is $2g$ dimensional. This is in correspondence between the previous setting which included g linearly independent curves, therefore, the $g + k - 1$ curves specify a genus g handlebody.

The α (resp. β) curves are pairwise disjoint, therefore $\Sigma \setminus \{\boldsymbol{\alpha}\}$ (resp. $\Sigma \setminus \{\boldsymbol{\beta}\}$) have k connected components. Let $\{A_i\}_{i=1}^k$ (resp. $\{B_i\}_{i=1}^k$) denote these components. Now, let $z_1, \ldots, z_k, w_1, \ldots, w_k$ be $2k$ basepoints on the surface disjoint from $\boldsymbol{\alpha}$ and $\boldsymbol{\beta}$, such that each connected component contains 2 basepoints, one from the z_i's and the other from the w_j's. Without loss of generality, after a relabeling, we can assume that for all $i = 1, \ldots, k$, $z_i, w_i \in A_i$ and $z_{\sigma(i)}, w_i \in B_i$ for some permutation σ on k letters. This data determines a link by a similar manner; connect z_i to w_i by a path in A_i, w_i to z by a path in B_i for all i. Pushing the paths in A_i's into the handlebody U_0, and the ones in B_i's into U_1, we get an l-component oriented link L, where l is an integer satisfying $l \leq k$. We say that the diagram $(\Sigma, \boldsymbol{\alpha}, \boldsymbol{\beta}, z_1, \ldots, z_k, w_1, \ldots, w_k)$ is a $2k$-pointed Heegaard diagram compatible with

the link L.

In contrast with the previous sections, we will now work in the $g+k-1$ fold symmetric product of Σ. Then, the necessary definitions such as $\mathbb{T}_{\boldsymbol{\alpha}}$, $\mathbb{T}_{\boldsymbol{\beta}}$, intersection points, $\pi_2(\mathbf{x},\mathbf{y}), c(\phi)$ are all adapted in a straightforward way. In particular, $\mathbb{T}_{\boldsymbol{\alpha}}$ is now $\alpha_1 \times \ldots \times \alpha_{g+k-1}$.

3.3.2 Chain Complex

Consider again the intersection points between the tori $\mathbb{T}_{\boldsymbol{\alpha}}$ and $\mathbb{T}_{\boldsymbol{\beta}}$. Let $CFL^-_m(\Sigma,\boldsymbol{\alpha},\boldsymbol{\beta})$ be the free module generated by these intersection points over the polynomial algebra $\mathbb{F}_2[U_1,\ldots,U_k]$, where the subscript m stands for "multiple basepoints".

We give the generators the generalized versions of Maslov grading and Alexander filtration. The Maslov grading is generalized in a trivial way.

$$\begin{aligned} gr(\mathbf{x},\mathbf{y}) &= \mu(\phi) - 2\sum_{i=1}^{k} n_{w_i}(\phi) \\ gr(U_1^{m_1}\cdots U_k^{m_k}\cdot\mathbf{x},\ U_1^{j_1}\cdots U_k^{j_k}\cdot\mathbf{y}) &= gr(\mathbf{x},\mathbf{y}) + 2(j_1+\ldots+j_k) - 2(m_1+\ldots+m_k) \end{aligned}$$

Remember that Alexander filtration contains data about the link components. In Section 3.2, there was a one-to-one correspondence between w_i's and the link components. In this case, more than 1 basepoint may belong to the same link component. In order to deal with that problem, we relabel the basepoints in the following way. Let k_i denote the number of basepoints on the i^{th} link component, for $i = 1,\ldots,k$. Then, let S be the index set consisting of the pairs (i,j) such that $i \in \{1,\ldots,k\}$ and $j \in \{1,\ldots,k_i\}$ for fixed i. Then, Alexander filtration is defined by the following two equalities.

$$A(\mathbf{x}) - A(\mathbf{y}) = \left(\sum_{j=1}^{k_1}\left(n_{z_{1,j}}(\phi) - n_{w_{1,j}}(\phi)\right),\ \ldots\ ,\ \sum_{j=1}^{k_l}\left(n_{z_{l,j}}(\phi) - n_{w_{l,j}}(\phi)\right)\right)$$

$$A\left(U_{1,1}^{m_{1,1}}\cdots U_{1,k_1}^{m_{1,k_1}}\cdots U_{l,1}^{m_{l,1}}\cdots U_{l,k_l}^{m_{l,k_l}}\cdot\mathbf{x}\right) = A(\mathbf{x}) - (\sum_{j=1}^{k_1} m_{1,j}\ ,\ldots,\sum_{j=1}^{k_l} m_{l,j})$$

The second equality may be rephrased as, multiplication by $U_{i,j}$ drops the filtration level by $g(i)$, the i^{th} basis vector.

With this setting, there are various ways of defining knot and link invariants, simply by changing which disks to count [14]. First, let's consider the analogue of CFL^-, whose differential map is formed by counting disks disjoint from the subvarieties determined by

the basepoints z_j for all j. Let $d(\phi)$ denote $c(\phi)$ modulo 2, and let $\partial^- : CFL_m^-(\Sigma, \boldsymbol{\alpha}, \boldsymbol{\beta}) \longrightarrow CFL_m^-(\Sigma, \boldsymbol{\alpha}, \boldsymbol{\beta})$ be defined as

$$\partial^-(\mathbf{x}) = \sum_{\left\{\substack{\mathbf{y} \in \mathbb{T}_\alpha \cap \mathbb{T}_\beta \\ \phi \in \pi_2(\mathbf{x},\mathbf{y})} \mid \substack{\mu(\phi)=1 \\ n_{z_{i,j}}(\phi)=0 \ \forall (i,j) \in S}\right\}} d(\phi) \cdot \left(\prod_{(i,j)\in S} U_{i,j}^{n_{w_{i,j}}(\phi)} \right) \cdot \mathbf{y} \, .$$

It is clear that this map again drops the Maslov grading by 1 and preserves the Alexander filtration. Moreover, from [17], it results that this construction is a link invariant. Consequently, let $HFL_m^-(L)$ denote the homology of the chain complex $(CFL_m^-(\Sigma, \boldsymbol{\alpha}, \boldsymbol{\beta}), \partial^-)$.

Another invariant is obtained by counting all disks with Maslov index equal to 1. Let $CFL'_m(\Sigma, \boldsymbol{\alpha}, \boldsymbol{\beta})$ denote again the free module generated by these intersection points over the polynomial algebra $\mathbb{F}_2[U_1, \ldots, U_k]$. Define the differential map by

$$\partial'(\mathbf{x}) = \sum_{\left\{\substack{\mathbf{y} \in \mathbb{T}_\alpha \cap \mathbb{T}_\beta \\ \phi \in \pi_2(\mathbf{x},\mathbf{y})} \mid \mu(\phi)=1\right\}} d(\phi) \cdot \left(\prod_{(i,j)\in S} U_{i,j}^{n_{w_{i,j}}(\phi)} \right) \cdot \mathbf{y} \, ,$$

and let $HFL'_m(L)$ denote the homology of the complex $(CFL'_m(\Sigma, \boldsymbol{\alpha}, \boldsymbol{\beta}), \partial')$. This version is going to re-appear in Chapter 4, when we review the combinatorial approach.

It is sometimes more useful to make use of the simpler complex $\left(\widehat{CFL}_m(\Sigma, \boldsymbol{\alpha}, \boldsymbol{\beta}), \partial\right)$, where $\widehat{CFL}_m(\Sigma, \boldsymbol{\alpha}, \boldsymbol{\beta})$ is the free $\mathbb{F}_2$ module generated by the intersection points and ∂ is the endomorphism of $\widehat{CFL}_m(\Sigma, \boldsymbol{\alpha}, \boldsymbol{\beta})$ given by

$$\partial(\mathbf{x}) = \sum_{\left\{\substack{\mathbf{y} \in \mathbb{T}_\alpha \cap \mathbb{T}_\beta \\ \phi \in \pi_2(\mathbf{x},\mathbf{y})} \mid \substack{\mu(\phi)=1 \\ n_{w_{i,j}}(\phi)=n_{z_{i,j}}(\phi)=0 \ \forall (i,j) \in S}\right\}} d(\phi) \cdot \mathbf{y} \, .$$

Let $\widehat{HFL}_m(L)$ denote the homology of the complex $\left(\widehat{CFL}_m(\Sigma, \boldsymbol{\alpha}, \boldsymbol{\beta}), \partial\right)$[17].

Theorem 3.1 conveys the relation between classical link Floer homology and link Floer homology with multiple basepoints. We are unable to provide proof for this theorem due to its depth of technical details. Later, we will establish the connection between link Floer homology with multiple basepoints and the combinatorial link floer homology (see Theorem 4.1), and consequently we will have a bridge connecting classical and combinatorial link Floer homology.

Theorem 3.1. *[8][1] Let $(\Sigma, \boldsymbol{\alpha}, \boldsymbol{\beta}, z_1, \ldots, w_k)$ be a $2k$-pointed Heegaard diagram for the l-component link L, with k_i pairs of basepoints for the i^{th} link component for all $i = 1, \ldots, l$.*

Then, there are multi-graded identifications

$$\widehat{HFL}_m(L) \cong \widehat{HFL}(L) \otimes \bigotimes_{i=1}^{l} V_i^{\otimes(k_i-1)} ,$$

where V_i is the 2 dimensional vector space spanned by one generator in Maslov grading and Alexander filtration zero, and another in Maslov grading -1 and Alexander filtration corresponding to $-g(i)$.

Chapter 4

COMBINATORIAL APPROACH TO HEEGAARD FLOER KNOT AND LINK HOMOLOGIES

In this final chapter, we will present another way to construct knot and link Floer homologies, which is more pleasing to the eye. Essentially, the following could have been constructed independently from everything we have established up to this point, but then it would mean to overlook the bridge that led to the goal, which would then be somewhat mystical.

We will establish the results mostly for a general link, but the reader should know that when the link in hand is composed of a unique component (itself - a knot), everything boils down to knot Floer homology.

Recall Example 2.1. It presented the simplest genus 1 Heegaard decomposition of S^3. This will be our basic data throughout this chapter. More precisely, the underlying Heegaard surface of our decomposition will always be the torus.

4.1 Grid Diagrams

We will consider several α curves on the torus. Recall that these curves are not allowed to intersect each other. Hence, if all the curves are homologically nontrivial, there is only one possibility of placing them up to isotopy and renaming. Note that it is unnecessary to consider the case where there is a null-homologous curve. The case for the β curves is exactly similar. Consequently, visualizing the torus as a square with opposite sides identified, after some isotopy, the α and β curves will constitute a so-called *"grid diagram"*, in which the α curves are all horizontal and β curves are vertical.

Given a link L, we shall try to associate a "sufficiently nice" grid diagram, whose meaning will be clear soon. Let us specify a couple more notation valid for throughout this chapter; along the usual notations used up to this point, "l" will stand for the number of components for the link L, n will denote the number of α curves in the grid diagram. Note that from

now on, we will only be interested in grid diagrams with an equal number of horizontal and vertical curves, and this number will be called *"the grid number"* of the grid diagram. So, a grid diagram with grid number n has $n \times n$ cells.

Let there be a a grid diagram of grid number n, together with a collection of black and white dots on it, with the following properties;

- each dot lies in some cell
- there is at most one dot in any cell
- each horizontal strip contains exactly one black and one white dot
- each vertical strip contains exactly one black and one white dot

Such a grid diagram is called a *"toroidal grid diagram"*, referring to the fact that the horizontal (resp. vertical) edges of the grid are identified. However, for the sake of simplicity, we will use "a grid diagram" to refer to a toroidal grid diagram.

A grid diagram supports a link, obtained by connecting black and white dots lying in the same vertical (resp. horizontal) strip with a vertical (resp. horizontal) segment, and whenever two of those segments intersect, letting the vertical segment to overpass the horizontal one. The orientation is specified by orienting the vertical segments from the black dots to the white dots, and the horizontal segments from the white dots to the black dots. The conditions above guarantee that the segments add up to form a link. Figure 4.1 shows a grid representation of two trefoils linked together.

The starting point of the combinatorial approach is that we can find a grid diagram representing L with the above properties [8]. This is the point where the presence of a null-homologous curve on the Heegaard surface becomes uninteresting.

Let now L be an l-component link. By [2], any two grid diagrams representing the same link can be connected by a sequence of the following three moves.

- **Cyclic permutation**; permuting the rows and the columns of the grid diagram. This basically corresponds to changing the way the torus is cut to form a square. See figures 4.9 and 4.11.

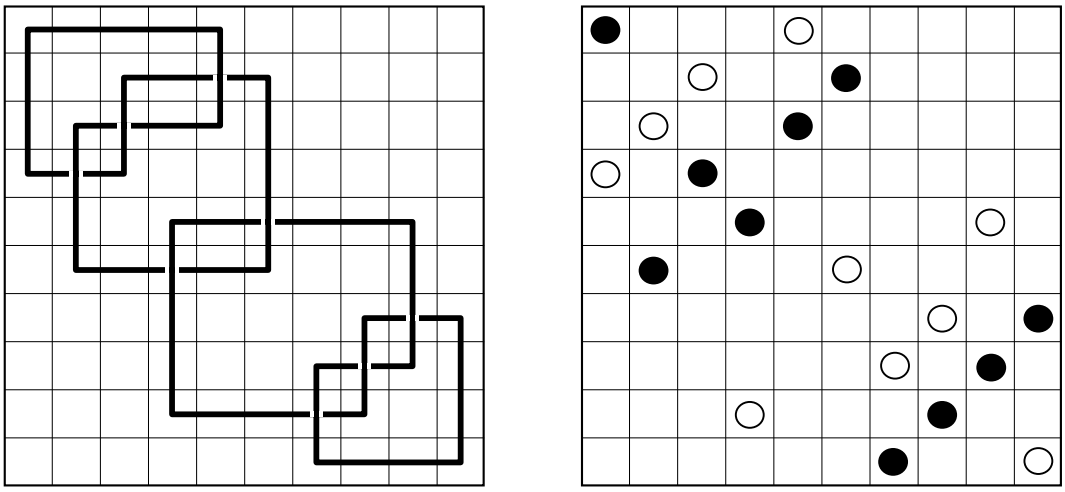

Figure 4.1: A grid diagram for a 2-component link with each component being a trefoil.

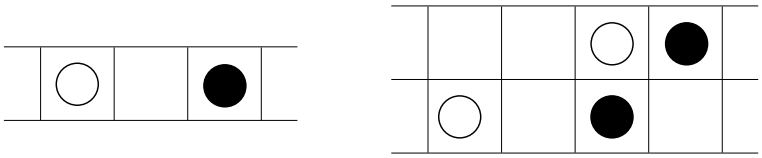

Figure 4.2: A stabilization move.

- **Commutation**; we can think of the black and white dot in a column as specifying a division of the vertical strip into two parts. Then, if both the black and the white dot in one of the adjacent column belong to the same part, we can interchange the two columns' decorations. Note that there is a similar move for rows.

- **Stabilization**; this is nothing but adding two consecutive breaks to a link component. This move adds one to the grid number of the diagram, i.e. inserts a new row and a column. See Figure 4.2

The algorithm we are about to review is independent from these moves, as proved in [7] using only combinatorial techniques. Independence from cyclic permutation will be easy to see once we prove propositions 4.1 and 4.2.

It turns out that it is possible to construct link Floer homology groups using only that

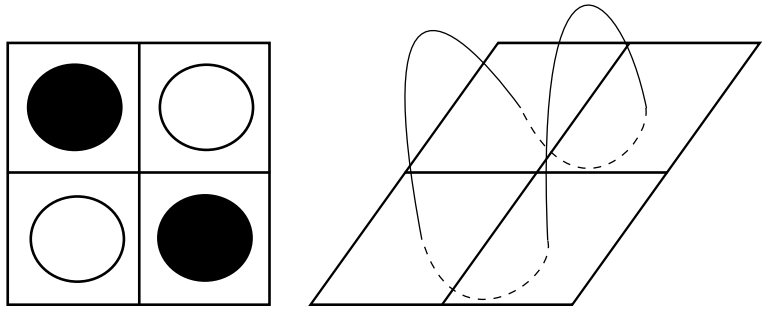

Figure 4.3: Constructing the link from the dots on the grid diagram.

grid diagram.

We remark that the dots in this setting correspond in some sense to basepoints in Chapter 3, because the black dots determine the point in the Heegaard surface (up to diffeomorphism of a square) where the link passes from U_0 to U_1. See Figure 4.3 for an illustration on the unknot.

4.2 The Chain Complex

From this point, we will work with grid diagrams, and construct a homology with $\mathbb{F}_2 = \mathbb{Z}/2\mathbb{Z}$ coefficients. We will later see that it will be equivalent to the link Floer homology of the previous chapter with coefficients reduced.

In link Floer homology, the generators were the intersection points in the symmetric product. Let us find out the analogue of an intersection point in the symmetric product in order to have a more clear idea about what the generators will be in the combinatorial case. Let $(x_1, \ldots, x_g)$ be an intersection point in $Sym^g(\Sigma)$. After some re-indexing of x_i's (which does not change the point itself by definition of the symmetric product) , we can assume that x_i belongs to α_i for all $i \in \{1, \ldots, g\}$. Then, there is a permutation σ in the symmetric group with g letters, such that $x_i \in \beta_{\sigma(i)}$ for all $i \in \{1, \ldots, g\}$. This is still true for the present case. Furthermore, in a grid diagram, any given α curve intersects any β curve at a single point. Therefore, the permutation σ uniquely determines the intersection point in a grid diagram. Hence, the generators of the chain complex will be in one-to-one correspondence with the permutations in g letters. See Figure 4.4. Given a grid diagram

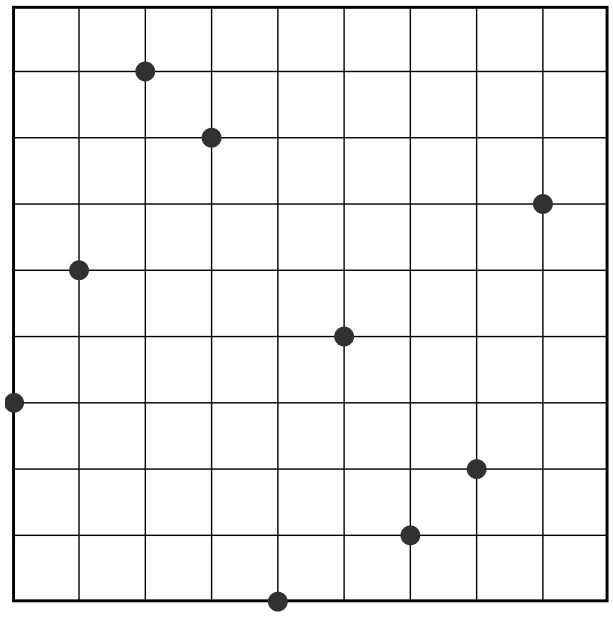

Figure 4.4: The generator corresponding to the permutation $\binom{123456789}{469815237}$.

Γ with grid number n, let P denote the set of intersection points, and consider the free $\mathbb{F}_2[U_1, \ldots, U_n]$ module generated by P, where $U_1, \ldots, U_n$ are n indeterminates. Each U_i is assigned to one of the n white dots via a one-to-one correspondence. We may denote the white dot assigned to U_i by w_i. We denote this module by $C^-(\Gamma)$. First, we endow $C^-(\Gamma)$ with a grading and a filtration, then we introduce the differential.

4.2.1 Grading and Filtration

The grading and the filtration described in this subsection will be the adaptations of the Maslov grading and the Alexander filtration of the previous chapter. However, the definitions will not be as straightforward as one might expect. We have to introduce an auxiliary function.

Note that throughout this subsection, we presume that among the identified top and bottom horizontal edges, only the bottom one is included in the diagram. Similarly, we omit the right vertical edge from the diagram in order to leave the left vertical edge as the only representative.

Given two finite collections of points $\mathcal{A}, \mathcal{B}$ in the grid diagram, we define $\mathcal{I}(\mathcal{A}, \mathcal{B})$ to be

the number of pairs $(a_1, a_2) \in \mathcal{A}$, $(b_1, b_2) \in \mathcal{B}$ such that $a_1 < b_1$ and $a_2 < b_2$. Then, define $\mathcal{J}(\mathcal{A}, \mathcal{B}) := (\mathcal{I}(\mathcal{A}, \mathcal{B}) + \mathcal{I}(\mathcal{B}, \mathcal{A}))/2$, and extend it bilinearly over formal sums of subsets.

Let now Γ be a grid diagram supporting an l-component link L. Let $\mathcal{Z}$, $\mathcal{W}$ denote the set of black and white dots in the grid diagram respectively. For a generator $\mathbf{x}$, we define the (absolute) Maslov grading as follows.

$$\begin{aligned} gr(\mathbf{x}) &= \mathcal{J}(\mathbf{x} - \mathcal{W}, \mathbf{x} - \mathcal{W}) + 1 \\ &= \mathcal{J}(\mathbf{x}, \mathbf{x}) - 2\mathcal{J}(\mathcal{W}, \mathbf{x}) + \mathcal{J}(\mathcal{W}, \mathcal{W}) + 1 \end{aligned}$$

Moreover, we define the filtration level $A(\mathbf{x}) = (A_1(\mathbf{x}), \ldots, A_l(\mathbf{x}))$ of the generator $\mathbf{x}$ in the following way.

$$A_i(\mathbf{x}) = \mathcal{J}(\mathbf{x} - \frac{1}{2}(\mathcal{Z} + \mathcal{W}), \mathcal{Z}_i - \mathcal{W}_i) + \frac{n-1}{2}$$

where $\mathcal{Z}_i, \mathcal{W}_i$ are the subsets of $\mathcal{Z}, \mathcal{W}$ corresponding to the i^{th} component of L [7]. It is seen that the filtration levels can also take half-integer values.

We also adopt the convention that multiplication by U_i drops the Maslov grading by 2, and the Alexander filtration level by the j^{th} basis vector if w_i belongs to the j^{th} link component. That is, the element $U_i^m \cdot \mathbf{x}$ has grading and filtration level

$$\begin{aligned} gr(U_i^m \cdot \mathbf{x}) &= gr(\mathbf{x}) - 2 \cdot m_i \\ A(U_i^m \cdot \mathbf{x}) &= A(\mathbf{x}) - m \cdot g(j). \end{aligned}$$

We may then decompose $C^-(\Gamma)$;

$$C^-(\Gamma) = \bigoplus_{d \in \mathbb{Z}, h \in \mathbb{Z}^l} C_d^-(\Gamma, h),$$

where $C_d^-(\Gamma, h)$ is generated by expressions $U_1^{m_1} \cdots U_n^{m_n} \cdot \mathbf{x}$, where

$$\begin{aligned} gr(U_1^{m_1} \cdots U_n^{m_n} \cdot \mathbf{x}) &= d \\ A(U_1^{m_1} \cdots U_n^{m_n} \cdot \mathbf{x}) &= h. \end{aligned}$$

A priori, it may seem that the grading and filtration levels depend on the choice of how the torus is cut to form a square. The propositions below show that this is not the case.

Proposition 4.1. *The Maslov grading is invariant under cyclic permutation.*

Proof. We can place the grid diagram in $\mathbb{R}^2$ with the following conventions. The bottom left corner is at the origin, and the side of each square has length 1, so that the top right corner has coordinates (n, n). The black and white dots on the diagram have half-integer coordinates.

Let Γ be a grid diagram, and Γ' be the one obtained by replacing the bottom strip on top of the top strip. Let $\mathbf{x}$ be the representation of a generator in Γ, and let $\mathbf{x}'$ be the same generator represented in Γ'. Similarly, let $\mathcal{W}$ and $\mathcal{W}'$ be the collection of white dots in Γ and Γ' respectively. We will show that $gr(\mathbf{x}) = gr(\mathbf{x}')$.

Now, there is a point x'_m with coordinates (m, n) in $\mathbf{x}'$. The corresponding point x_m is at $(m, 0)$ in $\mathbf{x}$. Other than that, the components of both representations are the same. Let x_i denote those components for $i \in \{0, \dots, \widehat{m}, \dots n\}$, where the hat denotes as usually an element omitted from the list, and the indices representing the horizontal projections. Similarly, $\mathcal{W}$ contains a point with coordinates $(l - \frac{1}{2}, \frac{1}{2})$. When forming $\mathcal{W}'$, the only modification is changing this point with $(l - \frac{1}{2}, n + \frac{1}{2})$.

For $m < i < n$, the pair (x_m, x_i) contributes 1 to $\mathcal{J}(\mathbf{x}, \mathbf{x})$, whereas the corresponding pair (x'_m, x_i) fails to do so for $\mathcal{J}(\mathbf{x}', \mathbf{x}')$. On the other hand, for $0 \leq i < m$, the pair (x_i, x_m) does not contribute to $\mathcal{J}(\mathbf{x}, \mathbf{x})$, but (x'_m, x_i) does add 1 to $\mathcal{J}(\mathbf{x}', \mathbf{x}')$. Therefore,

$$\mathcal{J}(\mathbf{x}, \mathbf{x}) = \mathcal{J}(\mathbf{x}', \mathbf{x}') + n - 2m - 1$$

Similarly, we find

$$\begin{aligned} 2\mathcal{J}(\mathbf{x}, \mathcal{W}) &= 2\mathcal{J}(\mathbf{x}', \mathcal{W}) + n - 2m \\ 2\mathcal{J}(\mathbf{x}', \mathcal{W}') &= 2\mathcal{J}(\mathbf{x}', \mathcal{W}) + 2l - n \\ \mathcal{J}(\mathcal{W}, \mathcal{W}) &= \mathcal{J}(\mathcal{W}', \mathcal{W}') - 2l + n + 1 \end{aligned}$$

Hence, we have obtained;

$$\begin{aligned} gr(\mathbf{x}) - 1 &= \mathcal{J}(\mathbf{x}, \mathbf{x}) - 2\mathcal{J}(\mathbf{x}, \mathcal{W}) + \mathcal{J}(\mathcal{W}, \mathcal{W}) \\ &= \mathcal{J}(\mathbf{x}', \mathbf{x}') - 2m + n - 1 - 2\mathcal{J}(\mathbf{x}', \mathcal{W}') + 2m + 2l - 2n \\ &\quad + \mathcal{J}(\mathcal{W}', \mathcal{W}') - 2l + n + 1 \\ &= \mathcal{J}(\mathbf{x}', \mathbf{x}') - 2\mathcal{J}(\mathbf{x}', \mathcal{W}') + \mathcal{J}(\mathcal{W}', \mathcal{W}') \\ &= gr(\mathbf{x}') - 1 \end{aligned}$$

Therefore, using the above argument repeatedly, we conclude that the grading is invariant under vertical rotation. The independence under horizontal rotation can be proved with a similar calculation. □

Proposition 4.2. *The Alexander filtration is invariant under cyclic permutation.*

Proof. Place the grid diagram Γ as in the proof of Proposition 4.1. Then, the intersection points of α and β curves correspond to points with integer coordinates. For such a point p, the numbers $\mathcal{I}(\mathcal{Z}_i - \mathcal{W}_i,\ p\ )$ and $\mathcal{I}(\ p\ , \mathcal{Z}_i - \mathcal{W}_i)$ both give the winding number of the i^{th} component around p.

Suppose p is an intersection point with first coordinate being in between the first coordinates of the black and white dots in the bottom horizontal strip. Then, when the bottom strip is replaced by a new one added on top of the diagram, the winding number will be changed by ± 1 according to the orientation of the link component. The only complication in verifying this may be for the case where the intersection point is on the very bottom of the diagram, but keep in mind that when the new strip is added, that very point is also carried onto the bottom of the new strip. Since the old winding number was zero, and the new one is ± 1, the same change takes place. On the other hand, if the point is outside the horizontal strip determined by the black and white dots, the winding number does not change. Furthermore, it is clear that for any other link component, the winding numbers stay the same.

Whereas for a point q with half-integer coordinates, it may be possible for a black or white dot to lie on q, so the number $\mathcal{I}(\mathcal{Z}_i - \mathcal{W}_i,\ q\ )$ is not necessarily the winding number around q. Anyhow, it is easy to see that it is always equal to the winding number of the i^{th} link component around the point $(q - \frac{1}{2}, q - \frac{1}{2})$. Similarly, $\mathcal{I}(\ q\ , \mathcal{Z}_i - \mathcal{W}_i)$ is nothing but the winding number around the point $(q + \frac{1}{2}, q + \frac{1}{2})$.

We recall here for convenience that $A_i(\mathbf{x}) - \frac{n-1}{2} = \mathcal{J}(\mathbf{x} - \frac{1}{2}(\mathcal{Z} + \mathcal{W}), \mathcal{Z}_i - \mathcal{W} - i)$. Suppose that there are m vertical segments between the black and white dots to be replaced. Then, there are m components of $\mathbf{x}$ for which the winding number will be changed by ± 1. The orientation of the link is constant, so the sign of the change is the same for every such point. So, the total change is $\pm m$. On the other hand, for each such vertical segment, $\mathcal{Z}$ and $\mathcal{W}$ contributes a count of 2 intersection points. So, for a fixed segment, they contribute a

change of $-\frac{1}{2}(\pm 2)$. Counting the m segments, we find that the total contribution is $\mp m$. They cancel out, and we get the desired invariance result. A similar reasoning takes care of horizontal rotation. □

4.2.2 Differential Map

Now we are ready to proceed into providing the chain complex $C^-(\Gamma)$ a differential map. In order to do that, we will use analogues of the holomorphic representatives of Whitney disks connecting two intersection points.

Rectangles

Let r be a rectangle in Γ whose edges are 4 of the intersection points of α and β curves. We remark that r can be split into 2 or 4 sub-rectangles if it is cut up while forming the grid diagram out of the torus Σ. Let $\mathbf{x}$, $\mathbf{y}$ be two generators. We say that r connects $\mathbf{x}$ to $\mathbf{y}$ if all but two of the components of $\mathbf{x}$ and $\mathbf{y}$ are the same, the remaining 4 components are the vertices of r, r is traversed by the orientation induced from that of Γ (that is, the boundary of r restricted to $\boldsymbol{\alpha}$ connects $\mathbf{y}$ to $\mathbf{x}$), and the horizontal components of r connects the component of $\mathbf{x}$ to the component of $\mathbf{y}$.

Definition. The set of all rectangles connecting $\mathbf{x}$ to $\mathbf{y}$ is denoted by $Rect(\mathbf{x},\mathbf{y})$. A rectangle r is said to be *empty* if $Int(r)\cap\mathbf{x}=\emptyset$. The set of empty rectangles connecting $\mathbf{x}$ to $\mathbf{y}$ is denoted by $Rect^{\circ}(\mathbf{x},\mathbf{y})$.

Observe that if $\mathbf{x}$ and $\mathbf{y}$ agree along all but two horizontal segments, then $Rect(\mathbf{x},\mathbf{y})$ has two rectangles. Otherwise it is empty. See Figures 4.5 and 4.6.

Differential

Given a pair of generators $\mathbf{x},\mathbf{y}\in C^-(\Gamma)$ and a rectangle $r\in Rect^{\circ}(\mathbf{x},\mathbf{y})$, we define $w_i(r)$ to be the number of times w_i appears in $Int(r)$. We endow the module $C^-(\Gamma)$ with the map $\partial^-: C^-(\Gamma)\longrightarrow C^-(\Gamma)$ defined as follows.

$$\partial^-(\mathbf{x})=\sum_{\{\mathbf{y}\in P\}}\sum_{\{r\in Rect^{\circ}(\mathbf{x},\mathbf{y})\}}U_1^{w_1(r)}\cdots U_n^{w_n(r)}\cdot\mathbf{x}.$$

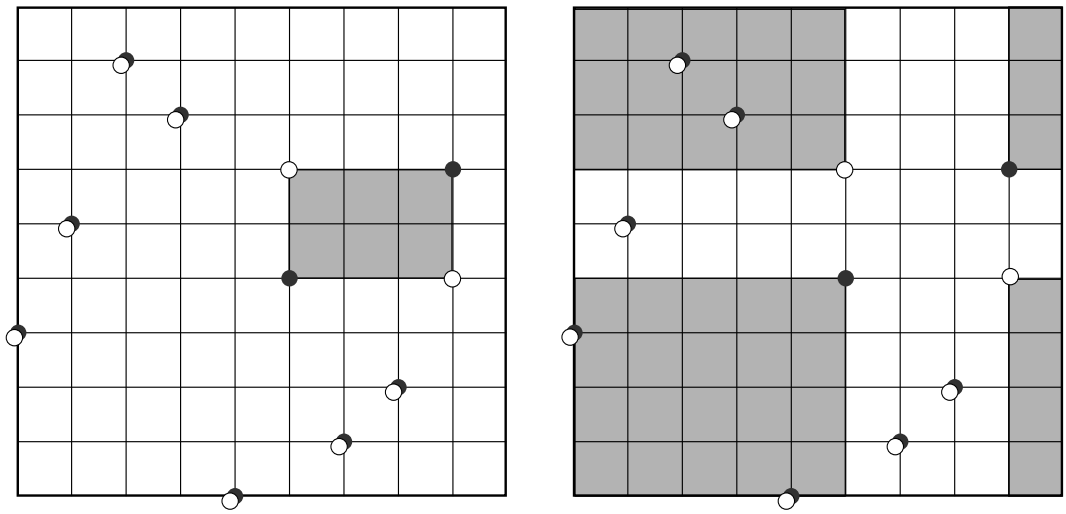

Figure 4.5: The small dark circles are the generator $\mathbf{x}$ and the hollow ones are $\mathbf{y}$. The two rectangles in $Rect(\mathbf{x}, \mathbf{y})$ are presented with a dark shading. The rectangle on the left is empty, whereas the one on the right is not.

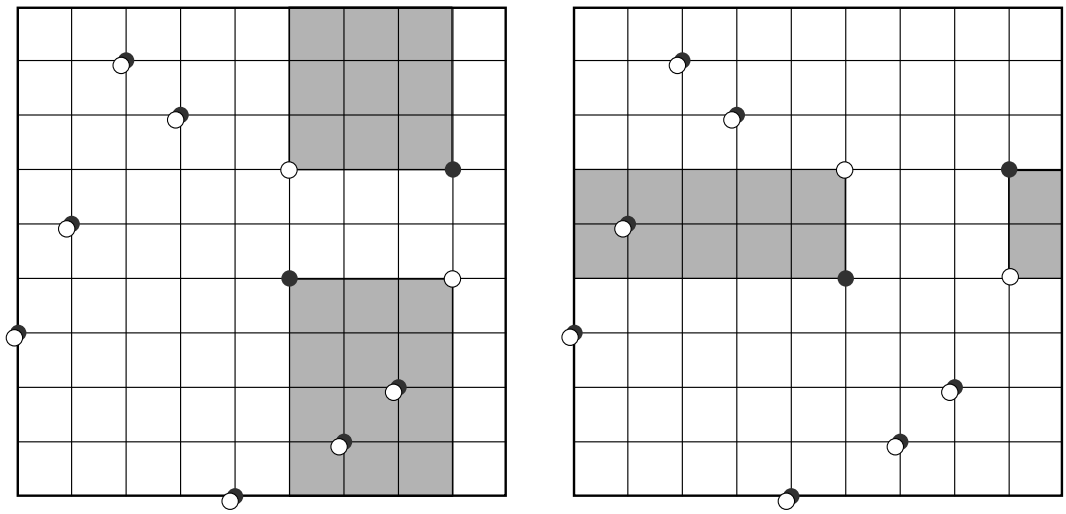

Figure 4.6: The two rectangles in $Rect(\mathbf{y}, \mathbf{x})$. Neither of them is empty.

We will verify that the square of this map vanishes. Before that, we will see the relation of ∂^- with the Maslov grading and the Alexander filtration.

Proposition 4.3. *Let $\mathbf{x} \in C^-(\Gamma)$ be a generator. Then, $\partial^-(\mathbf{x})$ is either zero or a sum of elements with Maslov grading $gr(\mathbf{x}) - 1$.*

Proof. Let $\mathbf{y}$ be a generator such that $Rect^\circ(\mathbf{x}, \mathbf{y})$ is nonempty, and let $r \in Rect^\circ(\mathbf{x}, \mathbf{y})$. Then, form the grid diagram in such a way that the lower left corner of r coincides with the lower left corner of the diagram. By Proposition 4.1, the gradings are independent of this choice. Recall that $gr(\mathbf{x}) = \mathcal{J}(\mathbf{x}, \mathbf{x}) - 2\mathcal{J}(\mathcal{W}, \mathbf{x}) + \mathcal{J}(\mathcal{W}, \mathcal{W}) + 1$.

In this setting, it is obvious that $\mathcal{J}(\mathbf{x}, \mathbf{x}) = \mathcal{J}(\mathbf{y}, \mathbf{y}) + 1$, the difference arising from the different pair of components. Moreover, $\mathcal{I}(\mathcal{W}, \mathbf{x}) = \mathcal{I}(\mathcal{W}, \mathbf{y}) + \#\{r \cap \mathcal{W}\}$, since the only difference is that for $w_i \in r$, the pair (w_i, x_k) adds one to $\mathcal{I}(\mathcal{W}, \mathbf{x})$ where x_k is the upper right corner of r. Similarly, the lower left corner comes into play for $\mathcal{I}(\mathbf{x}, \mathcal{W})$ and we have $\mathcal{I}(\mathbf{x}, \mathcal{W}) = \mathcal{I}(\mathbf{y}, \mathcal{W}) + \#\{r \cap \mathcal{W}\}$.

Plugging these results in the definition of the grading, we get,

$$gr(\mathbf{x}) = gr(\mathbf{y}) + 1 - 2\sum_{i=1}^{n} w_i(r).$$

Finally,

$$\begin{aligned} gr(\mathbf{x}, U_1^{w_1(r)} \cdots U_n^{w_n(r)} \cdot \mathbf{y}) &= gr(\mathbf{x}, \mathbf{y}) + gr(\mathbf{y}, U_1^{w_1(r)} \cdots U_n^{w_n(r)} \cdot \mathbf{y}) \\ &= gr(\mathbf{x}, \mathbf{y}) + 2\sum_{i=1}^{n} w_i(r) \\ &= 1 \end{aligned}$$

□

Proposition 4.4. *Let $\mathbf{x} \in C^-(\Gamma)$ be a generator. Then, $\partial^-(\mathbf{x})$ is either zero or a sum of elements with filtration levels $\leq A(x)$. In other words, the map ∂^- respects Alexander filtration.*

Proof. Let again $\mathbf{y}$ be a generator such that $Rect^\circ(\mathbf{x}, \mathbf{y})$ is nonempty, and let $r \in Rect^\circ(\mathbf{x}, \mathbf{y})$. Assume the U_i belongs to the $f(i)^{th}$ link component for some $f : \{1, \ldots, n\} \longrightarrow \{1, \ldots, l\}$. By a similar analysis as in the proof of Proposition 4.3, it is not difficult to see that

$$A(\mathbf{x}) - A(\mathbf{y}) = \sum_{i=1}^{n} (z_i(r) - w_i(r)) \cdot g(f(i)) \ .$$

Here, z_i is a black dot which belongs to the same link component as w_i, and z_i is different from z_j if $i \neq j$. Compare the corresponding Alexander filtration formula in Subsection 3.3.2.

Therefore,

$$\begin{aligned} A(\mathbf{x}) - A(U_1^{w_1(r)} \cdots U_n^{w_n(r)} \cdot \mathbf{y}) &= A(\mathbf{x}) - A(\mathbf{y}) + A(\mathbf{y}) - A(U_1^{w_1(r)} \cdots U_n^{w_n(r)} \cdot \mathbf{y}) \\ &= \sum_{i=1}^{n} z_i(r) \cdot g(f(i)) \ \geq (0, \ldots, 0) \end{aligned}$$

□

Let's introduce a final useful definition concerning a generalization of rectangles, in order to ease our way in proving Proposition 4.5.

Definition. Given $\mathbf{x}, \mathbf{y} \in C^-(\Gamma)$, a *path* from $\mathbf{x}$ to $\mathbf{y}$ is a closed oriented path γ composed of arcs on α and β curves, with orientation dictated by the grid diagram Γ, and with corner points coinciding with components of $\mathbf{x}$ and $\mathbf{y}$. A *domain* p from $\mathbf{x}$ to $\mathbf{y}$ is a two chain in Γ, such that ∂p is a path γ from $\mathbf{x}$ to $\mathbf{y}$. Let $\pi(\mathbf{x}, \mathbf{y})$ denote the space of domains from $\mathbf{x}$ to $\mathbf{y}$.

Observe that for $p_1 \in \pi(\mathbf{x}, \mathbf{y})$, $p_2 \in \pi(\mathbf{y}, \mathbf{w})$, the concatenation $p_1 * p_2$ belongs to $\pi(\mathbf{x}, \mathbf{w})$. Furthermore, $w_i(p_1 * p_2) = w_i(p_1) + w_i(p_2)$.

Now we are ready to proceed in the proof of $\partial^- \circ \partial^- = 0$.

Proposition 4.5. *The map* $\partial^- : C^-(\Gamma) \longrightarrow C^-(\Gamma)$ *satisfies* $\partial^- \circ \partial^- = 0$.

Proof. It suffices to check the vanishing of ∂^{-2} on the generators. Let $\mathbf{x} \in C^-(\Gamma)$ be a generator. Observe that

$$\partial^- \circ \partial^-(\mathbf{x}) = \sum_{\{\mathbf{w} \in P\}} \sum_{\{p \in \pi(\mathbf{x}, \mathbf{w})\}} N(p) \cdot U_1^{w_1(r)} \cdots U_n^{w_n(r)} \cdot \mathbf{w} \ ,$$

where $N(p)$ counts modulo 2 the number of ways in which p can be decomposed into two rectangles $p = r_1 * r_2$ where $r_1 \in \mathit{Rect}^\circ(\mathbf{x}, \mathbf{y})$, $r_2 \in \mathit{Rect}^\circ(\mathbf{y}, \mathbf{w})$ for some generator $\mathbf{y} \in C^-(\Gamma)$.

Let now $\mathbf{w} \neq \mathbf{x}$ be a generator and $p \in \pi(\mathbf{x}, \mathbf{w})$ such that p can be decomposed into two empty rectangles. Then, we claim that there are exactly two ways of decomposing p into

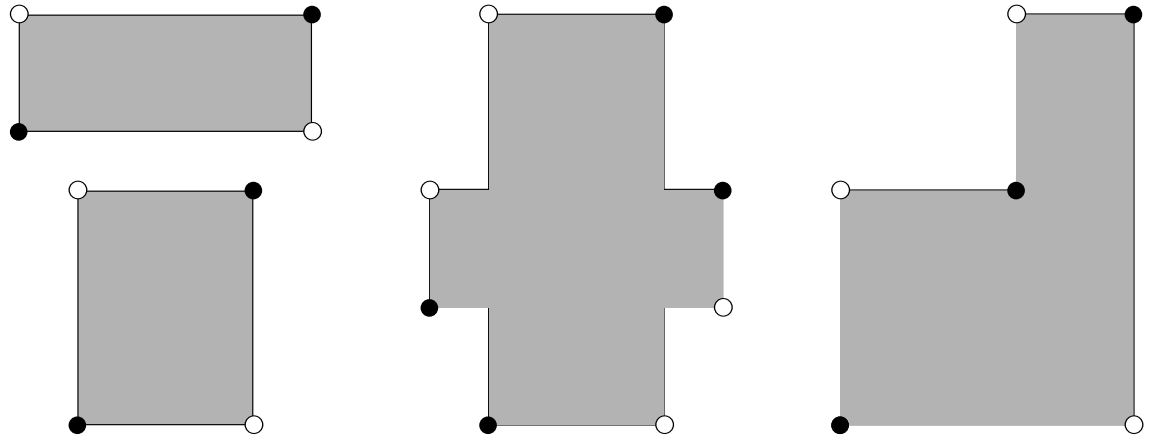

Figure 4.7: The 3 possible types of domains that can be decomposed as two empty rectangles, in the case where $\mathbf{x} \neq \mathbf{w}$.

two rectangles. Indeed, there are three possibilities for p, depicted in Figure 4.7. In the first two cases, the two orders in which rectangles are concatenated give 2 possible ways to recover p from the two rectangles. It is easy to see that there is no other way. It is also true for the third case, see Figure 4.8. Since we count modulo 2, the sum corresponding to these domains is therefore zero. We need finally to check for the domains connecting $\mathbf{x}$ to $\mathbf{x}$ that can be decomposed into two empty rectangles. Or, such a domain has to be an annulus. And if this annulus has height or width greater than 1, any decomposition will have at least one nonempty rectangle. Therefore, we consider height 1 horizontal and width 1 vertical annuli. On the other hand, any such annuli p has a unique decomposition $p = r_1 * r_2$, where $r_1 \in \pi(\mathbf{x}, \mathbf{y})$, $r_2 \in \pi(\mathbf{y}, \mathbf{w})$for fixed $\mathbf{y}$.

There are $2n$ such annuli, n vertical and n horizontal. Any given vertical annulus contributes $U_i \cdot \mathbf{x}$ to the differential for some i. But the vertical annulus corresponding to that U_i also contributes $U_i \cdot \mathbf{x}$, so in total, they cancel out to give zero. □

Therefore, the pair $(C^-(\Gamma), \partial^-)$ is a chain complex.

Definition. The homology of the chain complex $(C^-(\Gamma), \partial^-)$ is denoted by $H^-(\Gamma)$.

We remark here that although there are l link components, the free module $C^-(\Gamma)$ is generated over a polynomial algebra with n indeterminates, where $n > l$. But we have a

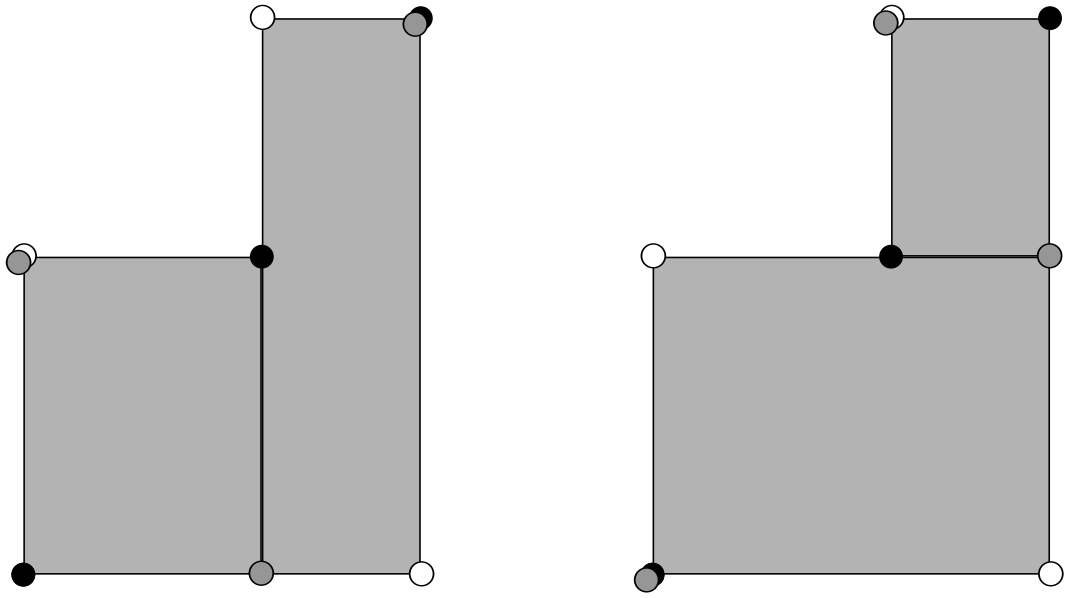

Figure 4.8: The 2 possible decompositions of the third domain type into two empty rectangles. The gray dots in the figures stand for two (different) auxiliary generators.

result proved in the next proposition linking the indeterminates corresponding to the same link component.

Proposition 4.6. *Suppose that w_i and w_j belong to the same link component. Then, multiplication by U_i is filtered chain homotopic to multiplication by U_j.*

Proof. The composition of filtered chain homotopies is itself a filtered chain homotopy, therefore it is enough to check for w_i and w_j such that there exists z_k in the same row as w_i and same column as w_j. Then, define

$$\begin{aligned} H : C^-(\Gamma) &\longrightarrow C^-(\Gamma) \\ \mathbf{x} &\mapsto \sum_{\{\mathbf{y}\in P\}} \sum_{\left\{\substack{r\in Rect^\circ(\mathbf{x},\mathbf{y}) \\ z_k\in r}\right\}} U_1^{w_1(r)}\cdots U_n^{w_n(r)}\cdot \mathbf{y}\,. \end{aligned}$$

The map H counts only the rectangles containing z_k. Using similar decompositions as in the proof of Proposition 4.5, we find that $\partial^-\circ H + H\circ\partial^- = U_i - U_j$. Namely, all the domains on the left hand side have 2 decompositions, except the horizontal and vertical annuli, which contribute U_i and U_k since they are on the same row and column (respectively) as z_k. □

Corollary. *Suppose the link L in the diagram has l components, and relabel $\mathcal{W}=\{w_j\}_{j=1}^{n}$ so that w_i belongs to the i^{th} link component for $i=1,\dots,l$. Then, the filtered chain homotopy type of $C^-(\Gamma)$ viewed as a free module over $\mathbb{F}_2[U_1,\dots,U_l]$ is independent of the ordering of $\mathcal{W}$.*

There is also a simpler invariant (introduced in [8]), which corresponds to $\widehat{HFL}$ in the classical approach. First, we set $U_i=0$ for all i, and then we take the graded object associated to the Alexander filtration. Recall that

$$gr(C^-(\Gamma))=\bigoplus_{s\in\mathbb{Z}[\frac{1}{2}]} gr_s(C^-(\Gamma))\ ,$$

where $gr_s(C^-(\Gamma))$ is the submodule generated by the generators at filtration level s. Then, $gr(C^-(\Gamma))$ corresponds to the free $\mathbb{F}_2$-module generated by the intersection points, endowed with the differential

$$\tilde{\partial}\mathbf{x}=\sum_{\mathbf{y}\in P}\ \sum_{\left\{\substack{r\in Rect^{\circ}(\mathbf{x},\mathbf{y})\\ \mathcal{W}_i(r)=\mathcal{Z}_i(r)=0\ \ \forall i\in\{1,\dots,n\}}\right\}} \mathbf{y}.$$

Observe that here we do not count the empty rectangles intersecting with $\mathcal{Z}\cup\mathcal{W}$. It is clear that setting $U_i=0$ guarantees that the rectangles intersecting with $\mathcal{W}$ do not contribute to the differential. Moreover, those intersecting with $\mathcal{Z}$ are eliminated while taking the graded object; recall that in the proof of Proposition 4.4, we have proved that if there exists a rectangle r connecting $\mathbf{x}$ to $\mathbf{y}$, we have $A(\mathbf{x})-A(\mathbf{y})=(\mathcal{Z}_1(r),\dots,\mathcal{Z}_n(r))$. Hence, if r has a black dot in it, the contribution of $\mathbf{y}$ to the differential of $\mathbf{x}$ is killed when we pass to the graded object associated to Alexander filtration. To put it another way, not only the differential $\tilde{\partial}$ respects the Alexander filtration, but it also respects the filtration level.

The homology of this complex is denoted by $\tilde{H}(\Gamma)$. Observe, if we denote by $gr_{s,t}(C^-(\Gamma))$ the sub-subcomplex generated by the generators at filtration level s and at grading t, we have

$$\tilde{H}(\Gamma)=\bigoplus_{s\in\mathbb{Z}[\frac{1}{2}]}\bigoplus_{t\in\mathbb{Z}}\tilde{H}_{s,t}(\Gamma)\ ,$$

where the homology groups $\tilde{H}_{s,t}(\Gamma)$ are

$$\tilde{H}_{s,t}(\Gamma)=\frac{\ker\left(\tilde{\partial}_{s,t}:gr_{s,t}(C^-(\Gamma))\longrightarrow gr_{s,t-1}(C^-(\Gamma))\right)}{\mathrm{Im}\left(\tilde{\partial}_{s,t+1}:gr_{s,t+1}(C^-(\Gamma))\longrightarrow gr_{s,t}(C^-(\Gamma))\right)}\ .$$

4.3 Relation Between Combinatorial Link Floer Homology and Link Floer Homology with Multiple Basepoints

Recall that the grid diagram is a special case of a multiple-pointed Heegaard diagram (see the beginning of Section 3.3), so we can associate both homologies to such a diagram. The main result about these homologies is Theorem 4.1, but it uses the fact that the Alexander filtrations and Maslov gradings of both invariants are the same. For the proof of these identifications, see [8], Lemmas 3.1 and 3.2. We will take those granted in the next theorem, which states that combinatorial link Floer homology and link Floer homology with multiple basepoints are basically the same.

Theorem 4.1. [8] *Let Γ be a grid diagram with grid number n and $(\Sigma, \boldsymbol{\alpha}, \boldsymbol{\beta}, z_1, \ldots, w_n)$ be the associated $2n$-pointed Heegaard diagram, for the l-component link L, with k_i pairs of basepoints for the i^{th} link component for all $i = 1, \ldots, l$. Then, we have*

$$\tilde{H}(\Gamma) \;\cong\; \widehat{HFL}_m(L)$$

Consequently, using Theorem 3.1, we obtain the identification

$$\tilde{H}(\Gamma) \;\cong\; \widehat{HFL}(L) \otimes \bigotimes_{i=1}^{l} V_i^{\otimes(k_i-1)} \;,$$

where V_i is the 2 dimensional vector space spanned by one generator in Maslov grading and Alexander filtration zero, and another in Maslov grading -1 and Alexander filtration corresponding to $-g(i)$.

Proof. We assume that both homologies possess the same grading and filtration, so there should be no confusion when we write $A(\mathbf{x})$ or $gr(\mathbf{x})$ for any generator $\mathbf{x}$ in the grid diagram. Hence, it only remains to see that the differential maps are the same. Let then $\mathbf{x}$ be any generator. Explicitly, we want to prove

$$\sum_{\left\{\substack{\mathbf{y}\in P \\ \phi\in\pi_2(\mathbf{x},\mathbf{y})} \,|\, \substack{\mu(\phi)=1 \\ n_{w_{i,j}}(\phi)=n_{z_{i,j}}(\phi)=0 \;\; \forall (i,j)\in S}\right\}} d(\phi)\cdot\mathbf{y} = \sum_{\mathbf{y}\in P} \sum_{\left\{\substack{r\in Rect^{\circ}(\mathbf{x},\mathbf{y}) \\ w_i(r)=z_i(r)=0 \;\; \forall i\in\{1,\ldots,n\}}\right\}} \mathbf{y}.$$

In [8], the Maslov grading is defined using the relation

$$gr(\mathbf{x}) - gr(\mathbf{y}) = P_{\mathbf{x}}(D) - P_{\mathbf{y}}(D) - \sum_{i=1}^{n} w_i(D),$$

where D is any domain connecting $\mathbf{x}$ to $\mathbf{y}$, $P_{\mathbf{x}}(D) = \sum_{x \in \mathbf{x}} p_x(D)$, and $p_x(D)$ is defined as the number of the squares contained in D among the 4 squares surrounding x. We will use this relation without proving.

By Proposition 2.7, a Whitney disk $\phi \in \pi_2(\mathbf{x}, \mathbf{y})$ is uniquely determined by its domain, and such domains on the grid diagram are of the form

$$D(\phi) = \sum_{1 \leq i,j \leq n} a_{i,j} D_{i,j} \ ,$$

where $D_{i,j}$ is the square lying in the i^{th} vertical and j^{th} horizontal strip, and $a_{i,j}$ is equal to the algebraic intersection number $n_p(\phi)$ for some $p \in D_{i,j}$. This is because the boundary of ϕ is mapped on the α and β curves.

Assume now $\partial(D(\phi)) \cap \alpha_i = 0$ for all but one $i \in \{1, \ldots, n\}$. Then, it must be zero on all the α circles by the equality

$$\partial D(\phi) = \sum_{1 \leq i,j \leq n} a_{i,j} \partial D_{i,j} \ .$$

Hence, $D(\phi)$ is some formal sum of the vertical annuli. But then, $\mathbf{x} = \mathbf{y}$, and the Maslov index $\mu(\phi)$ is even in view of Proposition 2.8.

A similiar reasoning works for the β curves. Therefore, we can assume that $\partial D(\phi)$ is non-zero on α_{j_1}, α_{j_2}, β_{i_1} and β_{i_2}. But then, there are permutations σ and τ such that

$$1/2 \leq p_{(i_1,\sigma(i_1))}(D(\phi)) + p_{(i_2,\sigma(i_2))}(D(\phi)) \leq P_{\mathbf{x}}(D(\phi))$$
$$1/2 \leq p_{(i_1,\tau(i_1))}(D(\phi)) + p_{(i_2,\tau(i_2))}(D(\phi)) \leq P_{\mathbf{y}}(D(\phi))$$

but ϕ cannot intersect the subvarieties determined by the basepoints if it is counted in the differential, therefore $1 = \mu(\phi) = P_{\mathbf{x}}(D(\phi)) + P_{\mathbf{y}}(D(\phi))$ [8], so the inequalities above are all equal. Therefore, $D(\phi)$ is zero everywhere but on α_{j_1}, α_{j_2}, β_{i_1} and β_{i_2}. Hence, $D(\phi)$ is one of the two rectangles with vertices $(i_1, j_1), (i_1, j_2), (i_2, j_1), (i_2, j_2)$. It is seen at once that $D(\phi)$ is an empty rectangle, and no basepoints lie in its interior. We have proved that a disk with non-negative multiplicities and Maslov index equal to 1 must admit a domain in the form of an empty rectangle. Therefore, all the generators counted in the differential of link Floer homology with multiple basepoints are also counted in the differential of combinatorial link Floer homology. Conversely, suppose we are given an empty rectangle r connecting $\mathbf{x}$ to

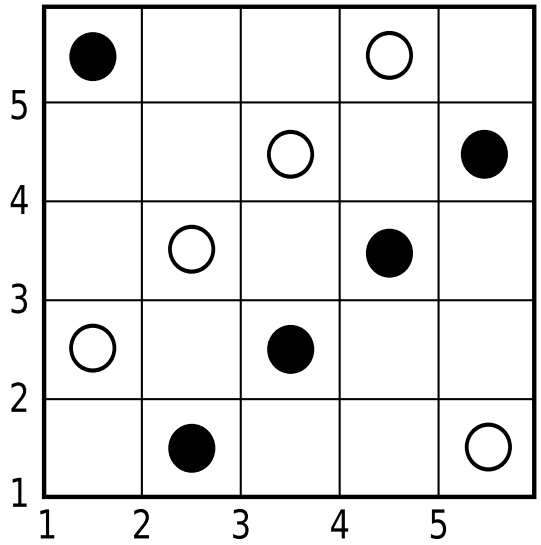

Figure 4.9: A grid diagram for the trefoil.

$\mathbf{y}$, containing no basepoints. In that case, it is proved in [8] that the number of pseudo-holomorphic representatives is odd, therefore $d(r) = 1$. Consequently, the two differentials are the same. The result follows from Theorem 3.1. □

Finally, we will work an example for the trefoil and the figure eight knot. However, the calculations for the homology $H^-(\Gamma)$ where Γ is a diagram for the trefoil are too extensive to carry out in the thesis, so we will calculate $\tilde{H}(\Gamma)$ which is easier to compute since it involves a fewer number of differentials.

4.4 Computation of $\tilde{H}$

4.4.1 Trefoil

In this section, we are going to compute $\tilde{H}(\Gamma_1)$ explicitly, where Γ_1 is the grid diagram for the trefoil depicted in Figure 4.9. The results without the calculations can also be found in [8]. Γ has grid number 5, therefore has $5! = 120$ generators. For the sake of simplicity, we will denote the generator consisting of the intersection of i^{th} horizontal segment with $\sigma(i)^{th}$ vertical segment as $(\sigma(1)\sigma(2)\sigma(3)\sigma(4)\sigma(5))$.

Recall that when computing $\tilde{H}(\Gamma)$, we are only interested in empty rectangles that are

also disjoint from $\mathcal{W}$ and $\mathcal{Z}$. Let's now list these rectangles by looking at which generators they connect. For instance, there is one such rectangle connecting the generator (12345) to (21345). First of all, it is seen at once that the only possible width, height values for these rectangles are, 1-by-1, 2-by-1 and 1-by-2.

Let's first classify 1-by-1 rectangles;

$$\begin{array}{lll}
(12**) \to (21**) & (34**) \to (43**) & (45**) \to (54**) \\
(*23**) \to (*32**) & (*45**) \to (*54**) & (*51**) \to (*15**) \\
(**12*) \to (**21*) & (**34*) \to (**43*) & (**51*) \to (**15*) \\
(***12) \to (***21) & (***23) \to (***32) & (***45) \to (***54) \\
(3***2) \to (2***3) & (4***3) \to (3***4) & (1***5) \to (5***1)
\end{array}$$

For every type of arrows above, there are $3! = 6$ differentials. In total, there are $15 \cdot 6 = 90$ arrows.

The 2-by-1 rectangles are of the form;

$$\begin{aligned}
(35**) &\to (53**) \\
(*41**) &\to (*14**) \\
(**52*) &\to (**25*) \\
(***13) &\to (***31) \\
(4***2) &\to (2***4)
\end{aligned}$$

So, there are 30 such rectangles. Finally, there also are 30 1-by-2 rectangles and they are;

$$\begin{aligned}
(**1*2) &\to (**2*1) \\
(3**2*) &\to (2**3*) \\
(*4**3) &\to (*3**4) \\
(4*5**) &\to (5*4**) \\
(*5*1*) &\to (*1*5*)\ .
\end{aligned}$$

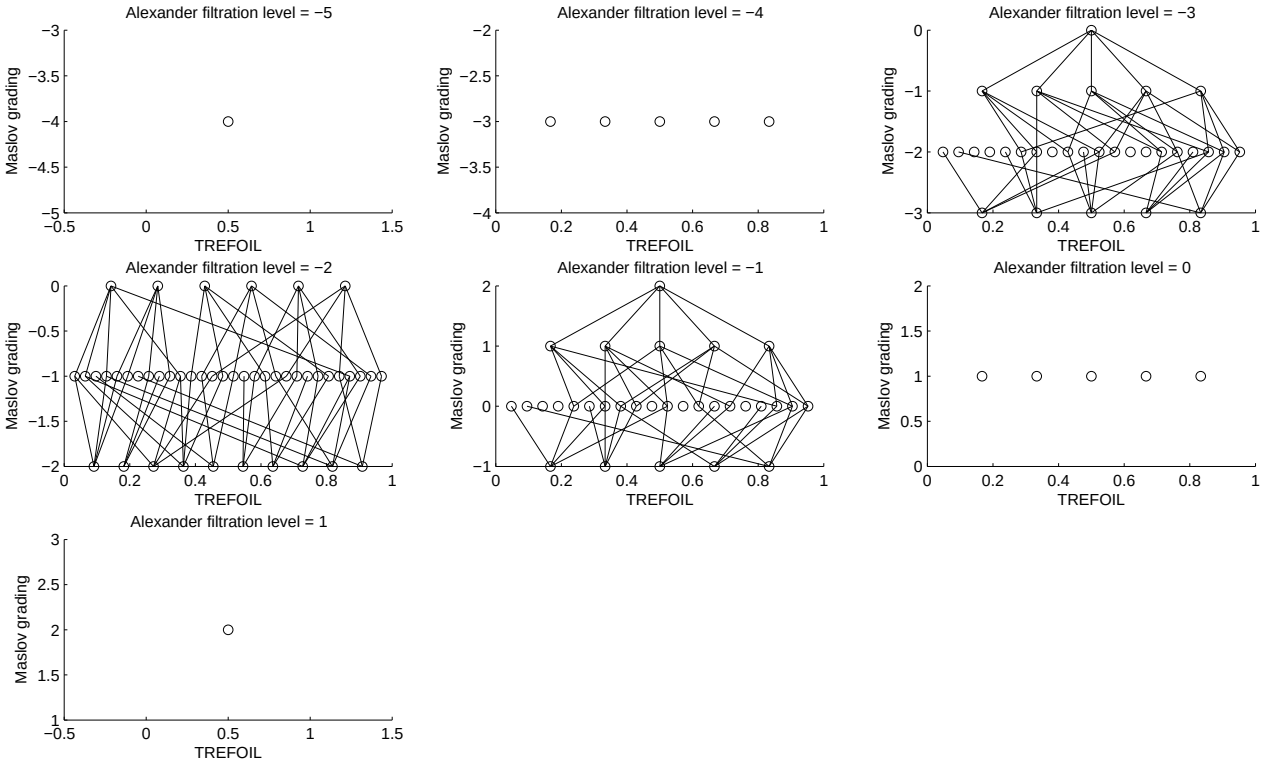

Figure 4.10: Chain complex for the grid diagram Γ_1 in Figure 4.9 representing the trefoil.

Using MATLAB, we compute the Maslov gradings and Alexander filtration levels for the generators, connect them with rectangles and plot the chain complex in Figure 4.10. The hollow circles correspond to generators, and the segments connecting two generators indicate that the generator below appears in the image of the generator above under the differential map. The homology ranks can be found in Table 4.1 below.

Note that our computations agree with the results presented in [8]. Moreover, let Γ_2 be the grid diagram for the trefoil presented in Figure 4.11. The computations result in the exact same homology rank table, consistent with the independence of the homology under cyclic permutation. The chain complex of Γ_2 is plotted in Figure 4.12.

4.4.2 Figure Eight Knot

A grid diagram for the figure eight knot is given in Figure 4.13. We may denote this grid diagram by Γ_3. This is the diagram presented in [7]. Similar to the trefoil case, we find

Rank of $\tilde{H}_{s,t}(\Gamma_1)$	$t=-4$	$t=-3$	$t=-2$	$t=-1$	$t=0$	$t=1$	$t=2$
$s=-5$	1	0	0	0	0	0	0
$s=-4$	0	5	0	0	0	0	0
$s=-3$	0	0	11	0	0	0	0
$s=-2$	0	0	0	14	0	0	0
$s=-1$	0	0	0	0	11	0	0
$s=0$	0	0	0	0	0	5	0
$s=1$	0	0	0	0	0	0	1

Table 4.1: Homology ranks for the trefoil. Γ_1 is presented in Figure 4.9. s stands for the Alexander filtration level, and t for the Maslov grading. Note that the ranks are zero at the half-integer valued filtration levels.

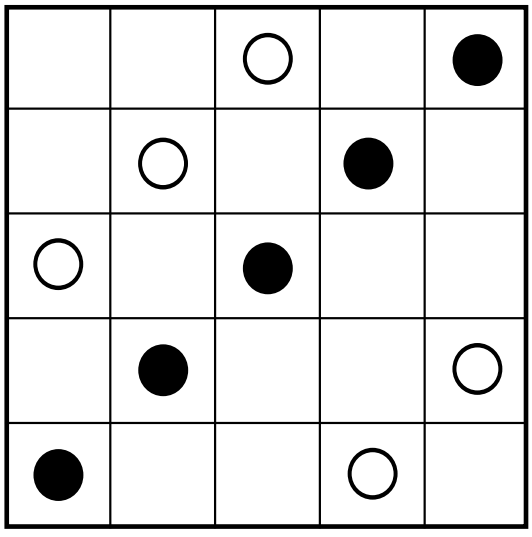

Figure 4.11: Another grid diagram for the trefoil, obtained by applying one horizontal cyclic permutation to Γ_1.

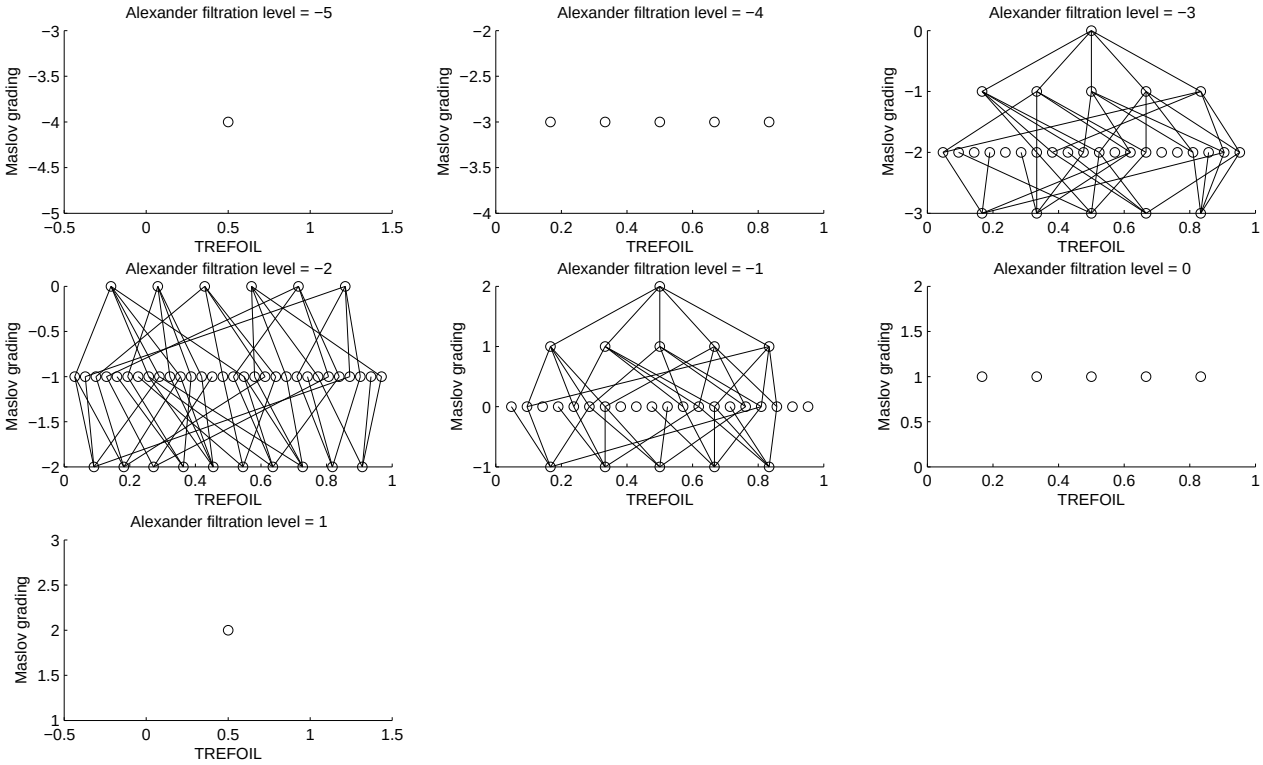

Figure 4.12: Chain complex for the grid diagram Γ_2 in Figure 4.11 representing the trefoil.

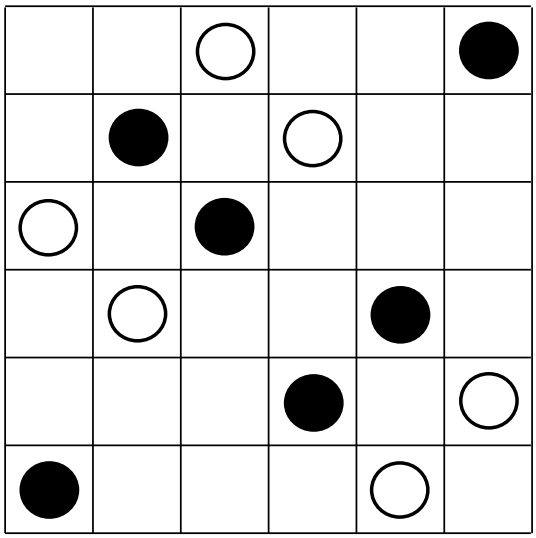

Figure 4.13: A grid diagram for the figure eight knot.

$6! = 720$ generators, and below is the list of types of empty rectangles, consisting of all 58 templates.

$$
\begin{array}{lll}
(23****) \to (32****) & (**12**) \to (**21**) & (****45) \to (****54) \\
(24****) \to (42****) & (**13**) \to (**31**) & (****46) \to (****64) \\
(2*3*\ast*) \to (3*2*\ast*) & (**14**) \to (**41**) & (****41) \to (****14) \\
(2**3**) \to (3**2**) & (**1*2*) \to (**2*1*) & (5***4*) \to (4***5*) \\
(34****) \to (43****) & (**23**) \to (**32**) & (6***4*) \to (4***6*) \\
(56****) \to (65****) & (**24**) \to (**42**) & (****56) \to (****65) \\
(51****) \to (15****) & (**34**) \to (**43**) & (****51) \to (****15) \\
(61****) \to (16****) & (**3*4*) \to (**4*3*) & (6***5*) \to (5***6*) \\
(6*1*\ast*) \to (1*6*\ast*) & (**56**) \to (**65**) & (*6**5*) \to (*5**6*) \\
(*12*\ast*) \to (*21*\ast*) & (***12*) \to (***21*) & (****61) \to (****16) \\
(*13*\ast*) \to (*31*\ast*) & (***34*) \to (***43*) & (2****1) \to (1****2) \\
(*1*2**) \to (*2*1**) & (***35*) \to (***53*) & (4****3) \to (3****4) \\
(*1*3**) \to (*3*1**) & (***45*) \to (***54*) & (5****3) \to (3****5) \\
(*1**2*) \to (*2**1*) & (***4*5) \to (***5*4) & (6****3) \to (3****6) \\
(*23*\ast*) \to (*32*\ast*) & (5**4**) \to (4**5**) & (*4***3) \to (*3***4) \\
(*2*3**) \to (*3*2**) & (***61*) \to (***16*) & (5****4) \to (4****5) \\
(*45*\ast*) \to (*54*\ast*) & (***62*) \to (***26*) & (6****4) \to (4****6) \\
(*61*\ast*) \to (*16*\ast*) & (***6*1) \to (***1*6) & (6****5) \to (5****6) \\
(*62*\ast*) \to (*26*\ast*) & (****23) \to (****32) & (*6***5) \to (*5***6) \\
(*63*\ast*) \to (*36*\ast*) \,. & & \\
\end{array}
$$

Consequently, there are $58 \cdot 4! = 1392$ rectangles. At this point we may remark that despite the fact that the grid number is grown by only 1, the numbers of generators and rectangles grow much more. In fact, our MATLAB code was unable to compute the homology rank table of Γ_3. Nevertheless, we presented the chain complex in Figure 4.14. We may notice once more the complexity of the algorithm by comparing figures 4.11 and 4.14.

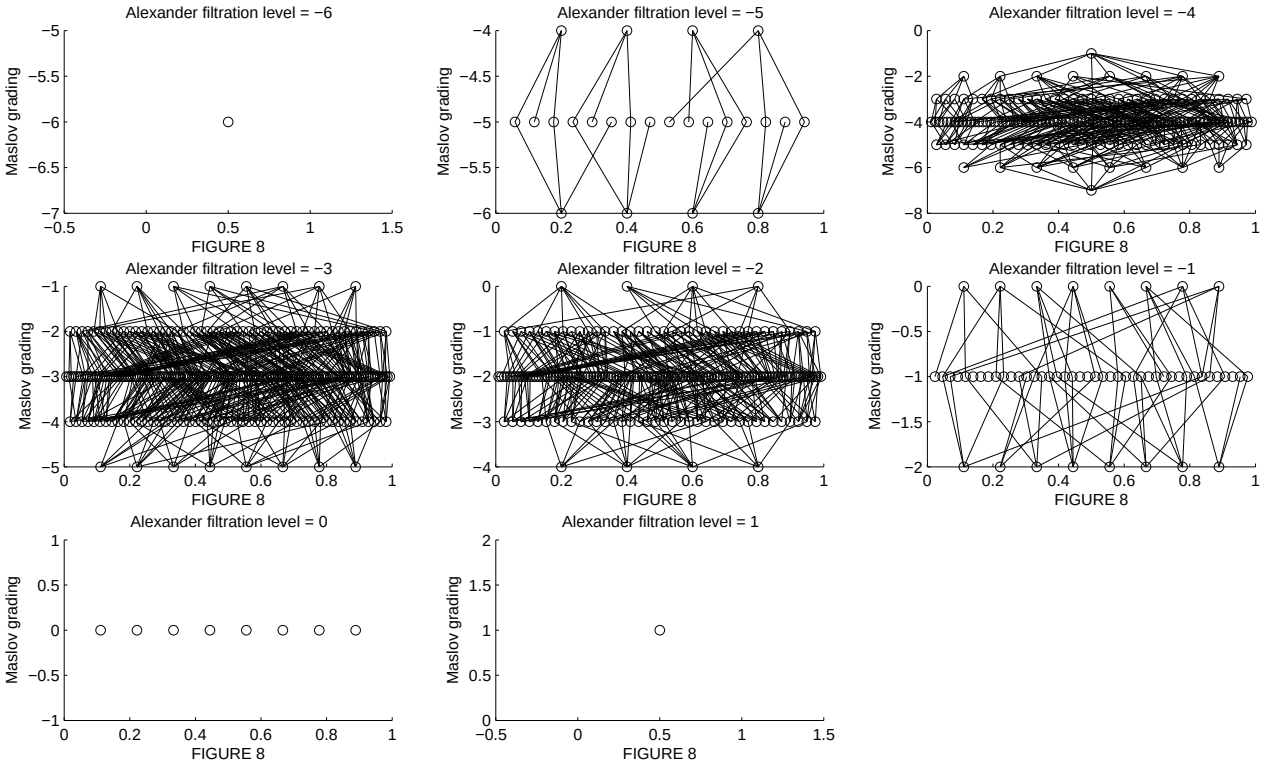

Figure 4.14: Chain complex for the grid diagram Γ_3 in Figure 4.13 representing the figure eight knot.

VITA

I, Taylan Bilal was born in Istanbul, Turkey on August 5, 1982. I received my B.Sc. degree in Industrial Engineering from Galatasaray University, in 2005. After one year in the Computational Sciences and Engineering Department of Koc University, I switched to the M.Sc. program in Mathematics.

BIBLIOGRAPHY

[1] A. Beliakova, "Simplification of Combinatorial Link Floer Homology", arXiv:0705.0669, 2007.

[2] P.R. Cromwell, "Embedding Knots and Links in an Open Book. I. Basic properties", *Topology Appl., 64(1995), no. 1*, 3758.

[3] A. Floer, "The Unregularized Gradient Flow of the Symplectic Action", *Comm. Pure Appl. Math*, 41(6):775-813, 1988.

[4] A. Floer, H. Hofer and D. Salamon, "Transversality in Elliptic Morse Theory for the Symplectic Action", *Duke Math. J*, 80(1):251-29, 1995.

[5] K. Fukaya, Y-G Oh, H. Ohta and K. Ono, "Lagrangian intersection Floer Theory - Anomaly and Obstruction", unpublished manuscript available at http://www.math.kyoto-u.ac.jp/ fukaya/fukaya.html, 2000.

[6] I.G. MacDonald, "Symmetric Products of an Algebraic Curve", *Topology*, 1:319-343, 1962.

[7] C. Manolescu, P. Ozsváth, Z. Szabó, D. Thurston, "On Combinatorial Link Floer Homology", *Geom. Topol. 11*, 2339–2412, 2007.

[8] C. Manolescu, P. Ozsváth, S. Sarkar, "A Combinatorial Description of Knot Floer Homology", arxiv:math/0607691, 2007.

[9] J. Milnor, "Morse Theory", *Princeton University Press*, 1963.

[10] K. Mulmuley, "A Fast Parallel Algorithm To Compute The Rank Of A Matrix Over An Arbitrary Field", *Combinatorica 7, no. 1*, 101–104, 1987.

[11] P. Ozsváth and Z. Szabó, "An Introduction to Heegaard Floer Homology", *Floer Homology, Gauge Theory, and Low-dimensional Topology, 3–27, Clay Math. Proc., 5, Amer. Math. Soc., Providence, RI*, 2006.

[12] P. Ozsváth and Z. Szabó, "Heegaard Diagrams and Floer Homology", *International Congress of Mathematicians. Vol. II, 1083–1099, Eur. Math. Soc.*, Zurich, 2006.

[13] P. Ozsváth and Z. Szabó, "Heegaard Diagrams and Holomorphic Disks", arXiv:math/0403029v1, *Different faces of geometry, 301–348, Int. Math. Ser. (N. Y.), 3, Kluwer/Plenum*, New York, 2004.

[14] P. Ozsváth and Z. Szabó, "Holomorphic Disks and Knot Invariants", math.GT/0209056, *Adv. Math. 186 (2004), no. 1*, 58–116, 2003.

[15] P. Ozsváth and Z. Szabó, "Holomorphic Disks and Three-Manifold Invariants: Properties and Applications", *Ann. of Math. (2)*, 159(3):1027-1158, 2004

[16] P. Ozsváth and Z. Szabó, "Holomorphic Disks and Topological Invariants for Closed Three-Manifolds", math.SG/0101206, *Ann. of Math. (2) 159 (2004), no. 3*, 1027–1158, 2003.

[17] P. Ozsváth and Z. Szabó, "Holomorphic disks, link invariants, and the multi-variable Alexander polynomial", math.GT/0512286, *Algebraic & Geometric Topology 8* (2008) 615692, 2005.

[18] J. Robbin and D. Salamon, "The Maslov Index for Paths", *Topology*, 32(4):827-844, 1993.